Nanoarchitectured Graphene-Based Supercapacitors for Next-Generation Energy-Storage Applications

Rahul R. Salunkhe, Ying-Hui Lee, Kuo-Hsin Chang, Jing-Mei Li, Patrice Simon, Jing Tang, Nagy L. Torad, Chi-Chang Hu, Yusuke Yamauchi

DOI: 10.1002/chem.201403649

Nanomaterials

Nanoarchitectured Graphene-Based Supercapacitors for Next-Generation Energy-Storage Applications

Rahul R. Salunkhe,[a, b] Ying-Hui Lee,[b] Kuo-Hsin Chang,[b] Jing-Mei Li,[b] Patrice Simon,[c] Jing Tang,[a, d] Nagy L. Torad,[a, d] Chi-Chang Hu,*[b] and Yusuke Yamauchi*[a, d]

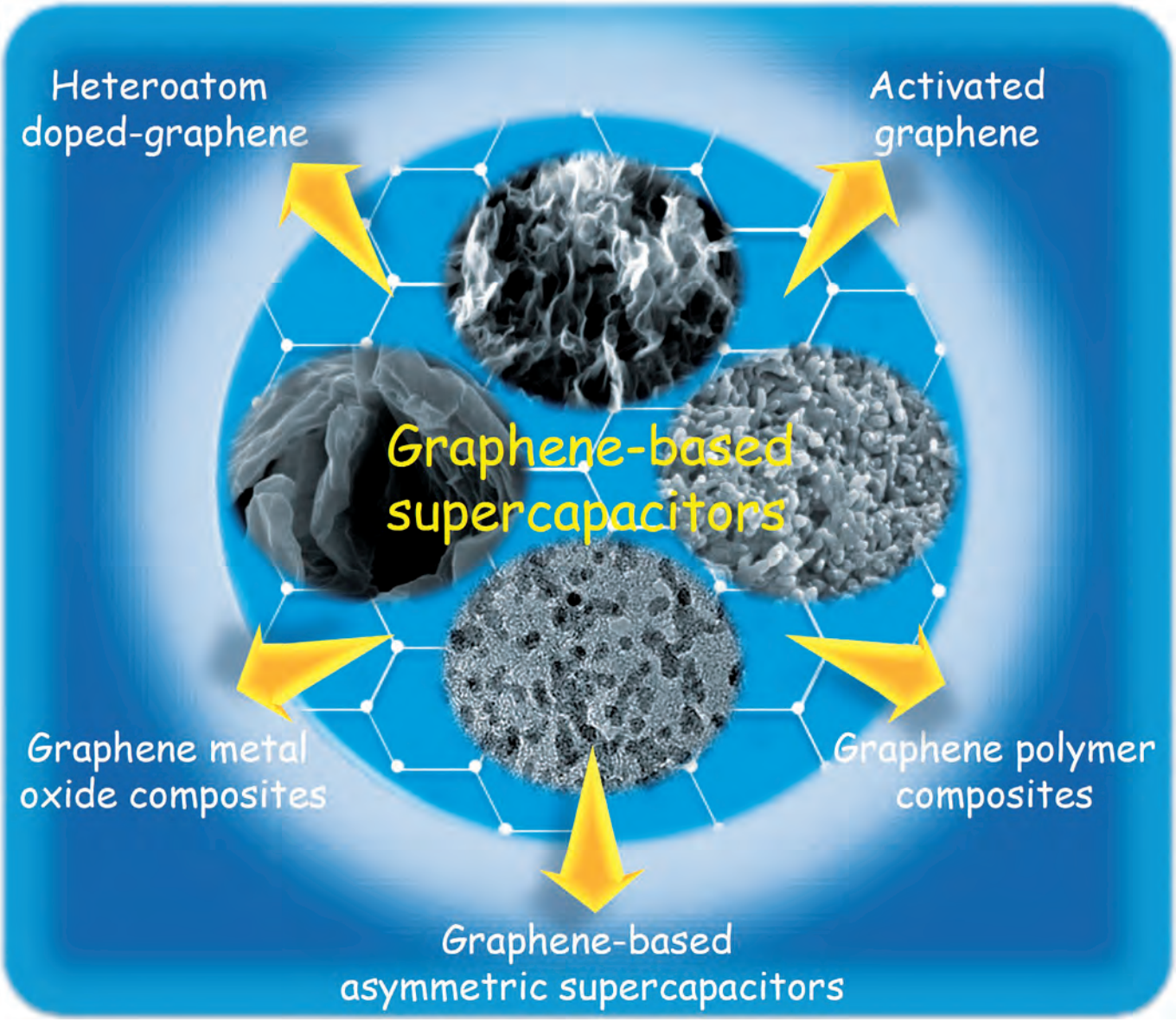

Abstract: Tremendous development in the field of portable electronics and hybrid electric vehicles has led to urgent and increasing demand in the field of high-energy storage devices. In recent years, many research efforts have been made for the development of more efficient energy-storage devices such as supercapacitors, batteries, and fuel cells. In particular, supercapacitors have great potential to meet the demands of both high energy density and power density in many advanced technologies. For the last half decade, graphene has attracted intense research interest for electrical double-layer capacitor (EDLC) applications. The unique electronic, thermal, mechanical, and chemical characteristics of graphene, along with the intrinsic benefits of a carbon material, make it a promising candidate for supercapacitor applications. This Review focuses on recent research developments in graphene-based supercapacitors, including doped graphene, activated graphene, graphene/metal oxide composites, graphene/polymer composites, and graphene-based asymmetric supercapacitors. The challenges and prospects of graphene-based supercapacitors are also discussed.

1. Introduction

Syntheses of various graphene materials with different shapes and the graphene composites have attracted considerable attention in development of energy-storage systems such as supercapacitors, batteries, and fuel cells. Currently, the development of cost-effective, maintenance-free, highly efficient, and environmentally friendly energy storage systems is becoming increasingly demanding. Among the various energy storage devices, supercapacitors are very attractive due to their high specific power ($>10\ kW\,kg^{-1}$) and moderate specific energy ($\approx 10\ W\,h\,kg^{-1}$).[1] These characteristics generally meet the growing demand for time-dependent electric power systems for portable electronics, hybrid electric vehicles (HEVs), power tools, stop-and-go systems, and others.[2] Consequently, designing a powerful energy-storage/delivery system with electrochemical capacitors (ECs) and developing next-generation ECs with much higher specific power and energy have become attractive research topics.

The applications of ECs in modern life can generally be divided into three types according to the power-supporting modes. As shown in Figure 1 a, ECs have been used in digital communication systems requiring pulses in milliseconds as well as in power tools and office machines with a peak-power time in seconds due to the unusual pulse–power property, acceptable energy density, and very long charge–discharge life cycle for ECs. Figure 1 b shows how ECs can efficiently capture

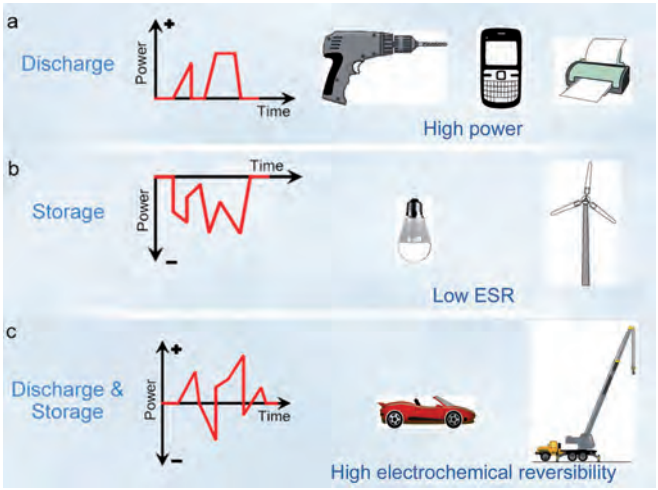

Figure 1. Typical power-supporting modes combined with ECs for various applications: a) power supply in the pulse/peak mode, b) efficient electricity leveling/capturing in electricity storage, and c) immediate power supply and recovery mode for stop-and-go systems.

and level fluctuating electricity generated from solar cells and wind power systems because of their relatively low equivalent series resistance (ESR), which significantly reduces the electricity loss and heat generation during the charging process. As clearly demonstrated in Figure 1 c, ECs provide an immediate power supply and recovery ability due to the ultrahigh reversibility of the CD process on electrode materials. Therefore, ECs have been considered as important energy-capture devices to increase the energy efficiency and save electricity in any go-and-stop systems, such as HEVs/EVs, load cranes, mass rapid transit (MRT), and elevators. In addition, EC researchers aim to increase energy and power densities, as well as lower fabrication costs by using environmentally friendly materials, for the increasingly important applications of ECs in power-management systems (e.g., smart grids).

The capacitance of supercapacitors generally comes from two energy-storage mechanisms: the electrical double-layer charge/discharge process and surface redox reactions of electroactive materials, which are used in the so-called EDLCs and (redox) pseudocapacitors, respectively.[3] In current EDLCs, carbon-based materials (such as activated carbon, AC) with high surface area have been mostly utilized as the electrodes.

[a] *R. R. Salunkhe, J. Tang, N. L. Torad, Prof. Dr. Y. Yamauchi*
World Premier International (WPI)
Research Center for Materials Nanoarchitectonics (MANA)
National Institute for Materials Science (NIMS)
1–1 Namiki, Tsukuba, Ibaraki 305-0044 (Japan)
E-mail: Yamauchi.Yusuke@nims.go.jp

[b] *R. R. Salunkhe, Y.-H. Lee, K.-H. Chang, J.-M. Li, Prof. Dr. C.-C. Hu*
Laboratory of Electrochemistry and Advanced Materials
Department of Chemical Engineering, National Tsing Hua University
Hsin-Chu 30013 (Taiwan)
E-mail: cchu@che.nthu.edu.tw

[c] *P. Simon*
CIRIMAT Laboratory (UMR CNRS 5085)
Department of Material Science, Université Paul Sabatier, Toulouse (France)

[d] *J. Tang, N. L. Torad, Prof. Dr. Y. Yamauchi*
Faculty of Science and Engineering, Waseda University
3-4-1 Okubo, Shinjuku, Tokyo 169-8555 (Japan)

The major contribution for the capacitance values comes from the charge accumulated at the electrode/electrolyte interface. Nanoporous carbons with high surface area are achieved through carbonization of metal–organic frameworks (MOFs) or porous coordination polymers (PCPs).[4] The resultant nanoporous carbons exhibit high electrochemical capacitances in an acidic aqueous electrolyte.[5] In contrast, a pseudocapacitor uses conducting polymers[6] or metal oxides[7] as an electrode material, which undergoes highly reversible Faradic redox reactions for electroactive species. Conducting polymers (e.g., polyaniline[6a,8] and polypyrrole[6b]) and metal oxides (e.g., RuO_2, MnO_2, NiO, and In_2O_3) have been shown to exhibit high pseudocapacitance but poor stability during charge–discharge cycling with the exception of RuO_2- and MnO_2-based materials.[9] Nickel and cobalt hydroxides with various shapes also exhibit high potential as novel electrochemical pseudocapacitors.[10] It is generally known that the typical charge–discharge times for pseudocapacitors are significantly longer than those of EDLCs. Carbon materials, such as activated carbons (ACs) and carbon nanotubes (CNTs), usually exhibit good stability but limited capacitance values. It is clear that EDLCs processes are surface phenomena, and hence the CD performance greatly depends on the electrolyte-accessible surface area. The micropores in carbon materials are inaccessible by the electrolyte, resulting in the inability of the double layer to form in the pores. This result leads to a decrease in the capacitance value (10–20% of the 'theoretical' capacitance) of ACs. Good electrical conductivity, high chemical and mechanical stability, and an optimized nanostructure are also other important factors that are responsible for achieving high capacitance values. In spite of the type of the charge storage mechanism, carbon-based materials are the most common materials for supercapacitor applications because of their outstanding properties such as their nontoxic nature, high electrical, chemical, and strong mechanical properties, and environmental friendliness, etc. The potential windows in nonaqueous electrolytes are generally larger than those obtained in aqueous media, although the overpotential of hydrogen evolution on carbons is high, especially in neutral electrolytes.

Recently, graphene has become a main research focus in the development of high-performance supercapacitors.[11] Graphene is an atomically thick, two-dimensional (2D) sheet consisting of sp^2-carbon atoms in a honeycomb network of six-member rings.[12] This material can be considered to be the basic unit for building all graphitic materials in various forms, such as zero-dimensional (0D) fullerenes, one-dimensional (1D) CNTs, and three-dimensional (3D) graphite (stacked graphene sheets). Besides this, graphene has shown high electrical conductivity, mechanical strength, and optical absorption properties that are clearly different from those of ACs, CNTs, and fullerenes, leading to the high research interest in physics and chemistry.[13] Other characteristics of graphene are its exceptionally high specific surface area of over 2600 $m^2 g^{-1}$, sufficient porosity, superior conductivity, a broad potential window, and rich surface chemistry.[1a,14] The major contributors to the specific surface area of graphene are not only the lateral sizes and their distribution in the solid state, but also the open porosity created between the graphene nanosheets. Because of these properties, graphene-based materials have been developed for high-power and high-energy supercapacitors, in order to circumvent the limitations to the power capability of supercapacitors caused by electrode kinetics, such as limited ion transport in the confined ultra-micropores of AC.

There have been several recent reviews on graphene-based electrode materials,[11,15] but at present there are no reviews focusing on certain important aspects, including the use of different dopants in graphene, the activation of graphene, as well as the use of graphene oxide for asymmetric supercapacitor applications. Thus, in this Review, we briefly address these aspects of the development of next-generation graphene supercapacitor electrodes. Also, a brief summary of recent progress in graphene-based electrode materials for supercapacitor applications is presented, including reduced graphene, activated graphene, doped graphene, graphene/metal oxide composites, graphene/polymer composites, and others. Their advantages and disadvantages are compared and summarized according to the literature available to date.

Chi-Chang Hu received his bachelor's degree in 1991 and Ph.D. in the Department of Chemical Engineering from National Cheng Kung University in 1995. After receiving his Ph.D., he worked at National Chung Cheng University as an assistant professor (1997), an associate professor (2000), and a full professor (2003). He joined National Tsing Hua University in 2007 and is presently working as a distinguished professor at the Department of Chemical Engineering, National Tsing Hua University. He has published about 200 SCI publications with the total number of citations more than 6200 and has an h-index of 41. He concurrently serves as an editorial board member for the Journal of the Taiwanese Institute of Chemical Engineers (indexed by SCI), an editorial advisory board member in the Open Electrochemistry Journal (indexed by SCI), and an editorial advisory board member in the International Journal of Electroactive Materials. His current research projects include the design of nanostructured materials for applications in supercapacitors, metal–air batteries, rechargeable metal–air batteries, organic electro-photocatalytic degradation, and solar water splitting.

Yusuke Yamauchi received his bachelor's degree in 2003, master's degree in 2004, and Ph.D. in 2007 from Waseda University in Japan. After receiving his Ph.D., he joined NIMS as permanent staff. Since 2008, he started his own research group 'Inorganic materials laboratory'. He has published more than 300 papers in international refereed journals with more than 5500 citations. He concurrently serves as visiting professor at several universities (Tianjin University in China, Waseda University in Japan), an associate editor of APL Materials published by the American Institute of Physics (AIP), and an editorial board member of Scientific Reports published by the Nature Publishing Group (NPG). His major research interest is tailored design of novel nanoporous materials with various shapes and compositions toward practical applications.

2. Electrode Materials Based on Graphene

R. S. Ruoff et al. reported a supercapacitor that uses chemically modified graphene.[16] With the high specific surface area of 705 $m^2 g^{-1}$, they obtain a specific capacitance of 135 $F g^{-1}$ (in aqueous electrolyte) and 99 $F g^{-1}$ (in organic electrolyte). C. N. R. Rao et al.[17] prepared reduced graphene-based materials with a high specific surface area of 925 $m^2 g^{-1}$, exhibiting a specific capacitance of 117 $F g^{-1}$ in aqueous H_2SO_4 electrolyte, but a high-temperature exfoliation process is difficult to control. Functionalized graphene sheets were prepared by low-temperature thermal exfoliation of a graphene sheet by J. Cao et al.,[18] which show a specific capacitance of 230 $F g^{-1}$ in KOH electrolytes. S. O. Kim et al.[19] reported on the development of 3D graphene platelets on flexible mesoporous carbon films, as shown in Figure 2a. These samples show a specific capacitance value of 86.7 $F g^{-1}$ in 1 M H_2SO_4 solution.

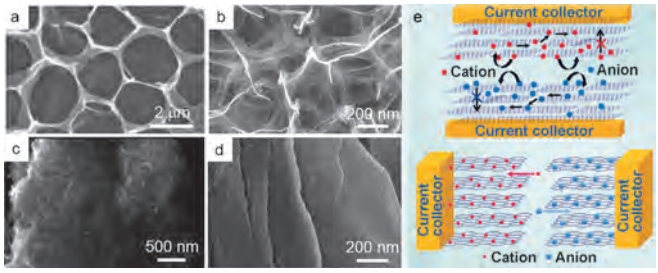

Figure 2. a) Plane-view SEM image of GO platelets self-assembled into mechanically flexible, macroporous 3D carbon films with tunable porous morphologies (reprinted from reference [19] with permission). b) SEM image of 3D graphene network by ethanol–CVD method (reprinted from reference [21] with permission). c) SEM image of 3D sponge graphene (reprinted from reference [22] with permission). d) SEM image of layered graphene structure (reprinted from reference [23] with permission). e) Schematic depiction of the stacked geometry used for the fabrication of supercapacitor devices and the operating principle of an in-plane supercapacitor device (reproduced from reference [32] with permission from the American Chemical Society).

Furthermore, B. Z. Jang et al.[20] developed a high-energy-density supercapacitor material based on graphene in an $EMIMBF_4$ ionic liquid electrolyte, which covered a very wide potential window of 4 V, leading to a high energy density of 85 $W h kg^{-1}$ at the current density of 1 $A g^{-1}$. H. Zhang et al.[21] reported the development of 3D structured materials on Ni foam using the chemical vapor deposition method for the supercapacitor application (Figure 2b). These composites show a very high specific capacitance of 816 $F g^{-1}$ with good rate capability. D. Mitlin et al.[22] reported the development of an ultrahigh energy density supercapacitor based on a sponge-like graphene nanoarchitecture, as shown in Figure 2c. These supercapacitors show an extremely high energy density of 48 $kW kg^{-1}$. Recently, our group has developed a layered graphene structure (Figure 2d), which showed a specific capacitance of 90 $F g^{-1}$ in 1 M H_2SO_4 electrolyte.[23]

S. J. Park et al.[24] reported polyaniline-coated multiwalled carbon nanotube–graphene sheet (MWCNT-GS) composites. By using the polyaniline coating, they improve the π–π interactions of all compounds. These samples show a high specific capacitance value of 1118 $F g^{-1}$ at a current density of 0.1 $A g^{-1}$. A very high specific surface area of 1654 $m^2 g^{-1}$ for graphene was obtained by F. Wei et al.,[25] although these samples show a specific capacitance of 254 $F g^{-1}$ with good rate capacity. The limitation for using such a method is that graphene with a high specific surface area cannot be produced on a large scale. Synthesis of a self-assembled graphene hydrogel was reported by a simple hydrothermal reduction method.[26] This graphene hydrogel has a well-defined 3D porous structure, demonstrating a specific capacitance as high as 240 $F g^{-1}$ at 1.2 $A g^{-1}$ in aqueous H_2SO_4 electrolyte. R. Kötz et al.[27] reported the effect of graphene layer spacing on the specific capacitance value. They obtain a specific capacitance of 220 $F g^{-1}$ for the graphene layer distance of 0.44 nm. The study reveals that the potential for anodic and cathodic electrochemical activation is a function of the graphene oxide (GO) layer distance. X. S. Zhao et al.[28] reported the intercalation of mesoporous carbon spheres between graphene sheets for supercapacitor applications. With the addition of mesoporous carbon spheres, the samples show an excellent electrical conductivity of 381 $S m^{-1}$, and the capacitance retention is improved up to 94% over 1000 CD cycles. C. C. Hu et al.[29] and Y. Chen et al.[30] independently reported CNTs as spacers of graphene nanosheets in order to avoid the restacking of graphene nanosheets, although the inhibition of graphene sheet restacking by adding MWCNTs has been employed to homogeneously disperse Pt nanoclusters with an improved electrocatalytic activity to the methanol oxidation.[31] The optimal mass ratio between MWCNTs and graphene sheets is 8:2, which shows a high specific capacitance value of 326 $F g^{-1}$. The 3D hierarchical architectures of MWCNT-GS composites reported by Chen's group show a specific capacitance of 318 $F g^{-1}$ with an energy density of 11 $W h kg^{-1}$. In another work by P. Ajayan et al.,[32] an 'in-plane' fabrication approach for ultrathin supercapacitors was reported based on electrodes composed of pristine graphene and multilayer reduced GO, as depicted in Figure 2e. The graphene-based 2D 'in-plane' supercapacitor shows a maximum specific capacitance value of 250 $F g^{-1}$, and the normalized capacitance reaches 394 $\mu F cm^{-2}$.

3. Electrode Materials Based on Activated Graphene

Generally, ACs are the most widely used electrode materials for EDLC applications because of their high specific surface area and relatively low cost. F. C. Wu et al. found that carbons activated with steam, KOH, and KOH + CO_2 exhibited high power, low ESR, and highly reversible characteristics.[33] The ACs prepared by the above methods generally show high supercapacitive performances in aqueous media, which are mainly attributed to the development of both mesopores and micropores. The highest surface area obtained is 2821 $m^2 g^{-1}$ (KOH activation and CO_2 gasification for 1 h). Recently, the concept of an activated GS has been proposed as a novel carbon electrode for EDLCs, which shows a 35% increase in the specific capacitance compared to pristine graphene nanosheets.[34] R. S. Ruoff

et al. reported that the specific surface area of the GS prepared by microwave exfoliation of GO was significantly enhanced to 3100 $m^2 g^{-1}$ after activation by KOH.[35] The schematic diagram for the chemical activation of graphene with KOH is shown in Figure 3. In this activated GS, there are large amounts of 0.6 to 5 nm wide pores in the highly curved, thin, sp^2-bonded carbon walls.

Figure 3. A scheme shows the microwave exfoliation/reduction of GO and the following chemical activation of GO with KOH. MEGO = microwave-exfoliated graphene oxide.

The activation treatment of an agglutinate GS not only increases its specific surface area but also creates short micropore channels that are significantly shorter than those in large AC particles. Therefore, an EDLC fabricated with activated GS electrodes exhibits excellent, high-power performance. For example, the activated GS-based EDLC maintains a rectangle-like CV behavior at a scan rate as high as 500 mV s^{-1} in an organic electrolyte. In addition, this device also possesses an energy density of 70 W h kg^{-1} and power density of 75 kW kg^{-1}, which are one order of magnitude higher than the values of AC-based EDLCs. Therefore, activated graphene sheets will make superior supercapacitors for energy storage in the future.

4. Electrode Materials Based on Graphene with Heteroatoms

The heteroatom doping of carbon materials has been demonstrated to give unique physicochemical properties, leading to superior capacitive performances by the change in electronic states of the graphene layer or the additional introduction of pseudocapacitance. The doping of different atoms, such as B,[36] N,[37] P,[38] and S,[39] into the carbon framework and the co-doping of these atoms[40] have been reported so far. The incorporation of B and N is more widely investigated, especially that of N; however, fewer studies show the effects of P and S on the carbon electrodes for EDLCs, because the larger size of these atoms limits their presence on the surface or edge of graphene as surface functional groups. On the other hand, since carbons are susceptible to oxidation during different preparation methods or treatments, surface oxygen-containing functional groups are ubiquitous and inevitable in almost every carbon material. Thus, oxygen incorporation is not included as a separate section in the following discussion.

4.1. Boron doping

The early B-incorporated carbons were obtained under a harsh environment. Boron was mixed with the carbon precursor and subject to extremely high temperatures (ca. 1800–3000 °C) to achieve doping in the graphitic structure through the diffusion of boron at such high temperatures.[36a,41] The high-temperature preparation leads to the formation of substituted B (188–189 eV), a B_4C structure (graphite-like structure, 186–187 eV), and B_2O_3 (192.5–193.5 eV).[36a,42] Recently, the carbonization of precursors employing either organic or organic/inorganic templates for B-doped carbons has also been reported, which form B–C (185–187 eV), B–O–C (192–192.2 eV), and B–O (191–193 eV).[36b,38b,43] In such self-assembly systems, boron is shown to prevent shrinkage of the templates and preserve the mesoporous structure to maintain the high specific surface area of the carbon materials.[38b,43] Compared to the extremely high temperature treatment that leads to a limited amount of boron (with the maximum of 2.5 at% doping at 2500 °C[44]), the B-impregnation during carbonization involving templates results in a boron content of up to 14 at%.[45]

The heteroatom doping of carbon materials will influence (a) the surface electronic states (i.e., double-layer capacitance), (b) the electric conductivity (i.e., capacitance retention), and (c) the types and amounts of functional groups on or within the graphene layers (i.e., pseudocapacitance). Accordingly, we discuss the effects of B doping in the following from the three perspectives.

The capacitance of EDLCs can be expressed by Equation (1)[46]:

$$\frac{1}{C} = \frac{1}{C_{SC}} + \frac{1}{C_H} + \frac{1}{C_{diff}} \quad (1)$$

in which C_{SC} is the space charge capacitance of the solid, C_H represents Helmholtz double-layer capacitance, and C_{diff} is the capacitance of the diffuse layer; the latter two belong to the electrolyte capacitance. Although the capacitance of an EDLC is usually determined by the high specific surface area of carbon materials, the capacitance would be limited when the surface area reaches 1200 $m^2 g^{-1}$.[47] The charge accommodation is restricted by the space constriction, especially for microporous carbon materials; that is, the capacitance is limited by the space charge capacitance of the solid. On the other hand, in concentrated electrolytes, C_{diff} is much larger than C_H, resulting in a negligible value of C_{diff}^{-1}. The value of C_H can be estimated to be 20 μF cm^{-2} for carbon materials in the absence of specific adsorption,[41] but the value of C_{SC} is relatively smaller,[48] establishing the dominant role of space charge capacitance for the measured capacitance considering the reciprocals of C_{SC} and C_H. The incorporation of boron has been demonstrated to enhance space charge capacitance to provide higher capacitance.[36,41] The substituted boron in the carbon framework would increase the number of holes as charge carriers due to its p-type characteristics, leading to the increase in charge carriers or the DOS (density of states) change at the Fermi level.[36,49] Then, the space charge capacitance is enhanced.[36,49] The influence of boron on the double-layer capacitance was further explored by a density functional theory (DFT) study on the zigzag edges of doped graphene nanoribbons (ZGNR) to reveal the ability of charge carriers to absorb

onto the B-doped carbons. The results showed that the larger critical distance for proton binding is obtained in comparison with N- and O-doped edges,[50] indicating easier proton binding on B-doped ZGNR, which correlates well with the higher interfacial capacitance for B-doped carbons reported in previous literature.[36,41] In addition, the maximum proton binding onto the substituted ZGNR was demonstrated to follow the rule of [8-*n*-1], where *n* represents the number of valence electrons of the substituted atom on the adsorption edge site.[51] Hence, among B-, N-, and O-doped ZGNRs, maximum proton loading can be achieved with boron substitution, further establishing the ability of B doping to enhance the interfacial capacitance.

Since B doping increases charge carrier concentration, the intrinsic electric conductivity of the doped carbons can be enhanced, leading to smaller ESR, which improves the capacitance retention during a fast charge–discharge process.[38b,41,43] The graphitic crystallinity (i.e., electric conductivity) grows as the concentration of B doping increases under extremely high temperature treatments, but only limited B doping can be achieved.[44] The capacitance retention is also determined by the porous structure of the electrodes. Ordered mesoporous structures fabricated by templates have been shown to be beneficial for electrolyte diffusion to promote capacitance retention.[36b,38b,40c,43] However, B doping introduces boron as defects in the ordered porous structure, increasing the charge transportation resistance for electrolytes in the pores. Consequently, the amount of B doping should be optimized for good electric conductivity while preventing the deterioration of the ordered porous structure for good capacitance retention.[43]

The B-doping results in B-containing functional groups on the graphene layers of carbons, such as substituted B, B_4C with a graphite-like structure, and B_2O_3, as mentioned in previous paragraphs. Functional groups on carbons are usually related to the contribution of additional pseudocapacitance. However, studies have shown that this is not the case for B-containing functional groups. Although the incorporation of boron has been demonstrated to enhance the space charge capacitance, the improvement of pseudocapacitance is ascribed to the abundant O-containing functional groups introduced simultaneously by B doping.[36b,38b,42,43] Several studies indicate that the incorporation of boron helps to bring in other heteroatoms such as oxygen or even nitrogen from the air at high temperatures, leading to broad redox peak responses at lower potentials.[42–44] Besides the increase of O-containing functional groups to provide pseudocapacitance by B doping, the resulting doped carbons also suppress the oxidation of carbon during the electrochemical analysis to stabilize the capacitive performance at high potentials, since the existence of a B–C bond lowers the Fermi level and tunes the chemisorption of oxygen.[38b,43,52] However, the inhibition to oxidation depends on the level of B doping and the position where the boron atom is being doped.[53] The low-level B doping (B/C less than ca. 0.7 %) actually shows a catalytic effect on the oxidation of carbons, whereas the inhibiting effect becomes dominant when more boron is introduced.[52] On the other hand, the study of B doping on different positions of either zigzag or armchair edges reveals that the preference of oxygen chemisorption is complicated and site dependent.[54] In addition to the pseudocapacitance, the enrichment of functional groups by B doping is thought to enhance the wettability of the doped carbons due to better hydrophilicity.[38b,40c,42,55] However, the contact angle tests for the droplets on the surface of pure, B-doped, and N-doped carbon-coated anodic aluminum oxide (AAO) yielded different results, as shown in Figure 4 a–f.[55] The

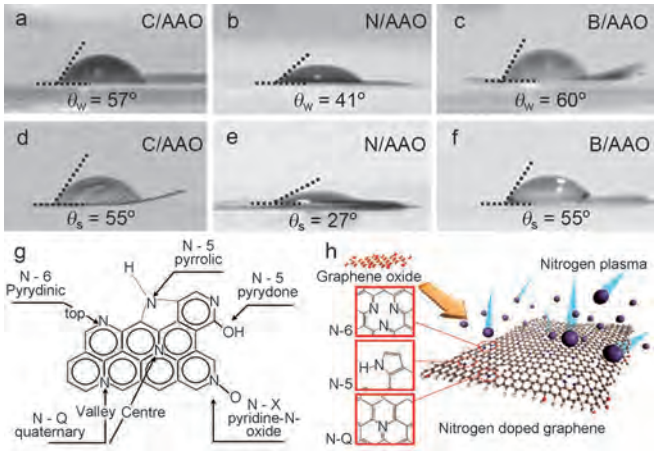

Figure 4. Graphene with heteroatoms. a–f) Photographs of a–c) water and d–f) 1 M H_2SO_4 droplets on the surface of pure carbon-coated AAO (C/AAO), N-carbon-coated AAO (N/AAO), and B-carbon-coated AAO (B/AAO), together with the corresponding contact angles (reprinted from reference [55] with permission). g) Four types of N-doped structures on graphene layers: pyridinic N (N-6), pyrrolic N/pyridine N (N-5), and quaternary N (N-Q), and pyridine-*N*-oxide (N-X) (reprinted from reference [59b] with permission). h) Illustration of nitrogen atoms replacing the existing carbon atoms on the basal plane during nitrogen-plasma treatment (reprinted from reference [37b] with permission).

pure and B- and N-carbon-coated AAO exhibit the same mesoporous structure, eliminating the effects of porosity on the contact between the electrolyte and the surface. It showed that only N-carbon-coated AAO displayed improved hydrophilicity in aqueous electrolytes. Although both water-vapor adsorption isotherms and droplet contact tests indicate that only N doping contributes to better wettability, B doping still demonstrates superior capacitive performances.[55] Accordingly, functional groups brought by B doping can enhance the pseudocapacitance, but improving the wettability of the doped carbons needs further study.

Due to the enhancement for double-layer capacitance and pseudocapacitance, the superior capacitive performances of B-doped carbons have been reported in both aqueous and nonaqueous electrolytes, in which the performances are compared by the interfacial capacitance ($F\,m^{-2}$) due to the relatively low specific surface area in most cases.[36,38b,42,43] With low-level B doping (B/C < 1 %), an interfacial capacitance of up to 0.3 $F\,m^{-2}$ can be obtained in an aqueous electrolyte, whereas it is 0.06–0.16 $F\,m^{-2}$ for ACs.[36b,44] However, the improvement is rather limited in nonaqueous electrolytes, which have values in the same range as ACs (i.e., 0.05–0.08 $F\,m^{-2}$). The ultimate goal

would be to develop B-doped graphene for EDLCs, combining the advantages introduced by B doping and the unique properties of graphene. However, thus far the preparations of B-doped graphene are few, and the utilization for EDLCs has not been reported to the best of our knowledge.[56] Yet, the successful employment of B-doped graphene as the anode for lithium-ion batteries[57] makes B-doped graphene a promising electrode for EDLCs in the near future. In addition, since the B doping helps bring other atoms into the graphitic structure during high-temperature treatment, the co-doping of boron and nitrogen or boron and phosphorus has also been demonstrated to exhibit positive effects on the capacitive performance.[40,44,45,58] The substituted boron in graphitic structures is preferentially bonded with nitrogen since the B–N bond is in the most stable energy state.[44] The presence of B–N is proposed to provide pseudocapacitance through the redox reaction with the proton,[40d] and even with a sodium ion and lithium ion for neutral electrolytes,[40d,45] which was confirmed by the larger current responses at lower potentials. On the other hand, the co-doping of boron and phosphorus was shown to introduce more O-containing functional groups to enhance the pseudocapacitance. The inhibition to hydrogen evolution at negative potentials and oxidation at highly positive potentials were also observed for the co-doping of B and P to stabilize the capacitive performance within the potential window.[40a,58] The contributions of nitrogen and phosphorus will be introduced in detail in the following sections.

4.2. Nitrogen doping

N doping is the most promising due to the well-established preparation methods. It can be achieved through the ammoxidation of certain carbon materials[59] and direct carbonization,[15a,60] hydrothermal/solvothermal treatments,[61] or chemical vapor deposition (CVD) treatments[37b,62] of nitrogen-containing precursors. Four types of nitrogen-containing functional groups have been found on graphene layers to enhance capacitive performance: pyridinic N (N-6, 398.5 eV), pyrrolic N/pyridine N (N-5, 400 eV), quaternary N (N-Q, 410.2 eV), and pyridine-*N*-oxide (N-X, 403 eV).[37a,63] As depicted in the left side of Figure 4g,[59b] N-6, N-5, and N-X structures are located on the edge of graphene, whereas N-Q appears either on the edge or on the basal plane of graphene. Since graphene layers are not always perfect, disruption on the basal planes is commonly observed, leading to the formation of N-6 and N-5 on the defects of the basal plane as well, as indicated by the right side of Figure 4h[37b] for the case of nitrogen-plasma treatment.

Similar to B doping, the incorporation of nitrogen changes the surface electronic property of graphene and enhances the double-layer capacitance of the doped carbons. The DFT (density functional theory) study for the proton adsorption on the doped edges indicates that proton exhibits stronger interactions with N-doped edges rather than B- or O-doped edges,[50] which may be ascribed to the increased basicity introduced by N-containing functional groups on the surface.[46,64] Different from the case for O-containing functional groups, which bear more acidic groups (e.g., carboxylic groups and lactones)[65] than basic and neutral groups (e.g., phenols, ethers, and carbonyls) to render acidic surface nature on carbons, the presence of N-containing functional groups introduces more basicity, especially for the ones containing high amounts of N-6 and N-5 due to their electron donor characteristics.[37a,63b] On the other hand, the DFT study also reveals that the type and the position (i.e., edge or basal planes) of N-containing functional groups influence the ion adsorption on the surface, showing that N-6 on the basal plane and anion N-5 on both basal and edge planes result in the larger binding energies for potassium ions on the electrode surface, which facilitates the formation of a double layer.[37b]

The electric conductivity of carbons can also be tuned by N doping. The presence of N-Q and N-X has been reported to enhance the electron transport through the carbon materials, maintaining superior capacitance retention during the fast charge–discharge process.[37a,63b] N-Q is proposed to lower the energy gap between the highest occupied molecular orbital (HOMO) and lowest unoccupied molecular orbital (LUMO), leading to improved electron transfer ability.[66] Such a phenomenon was confirmed by the high correlation coefficient (>0.97) between the specific capacitance and the amounts of N-Q and N-X when measured at high current loads.[37a,63b] However, the enhancement of electric conductivity is limited by the concentration of N doping. When the amount of nitrogen exceeds 12 at%, the electric conductivity starts decreasing due to the interruption of graphitic structure by N doping.[67]

In addition to the effects on double-layer capacitance and capacitance retention, the contribution of pseudocapacitance is the most important feature for N doping, as indicated in a previous study.[40c] N-6 and N-5 are believed to provide pseudocapacitance through redox reactions involving protons.[37b,66,68] The presence of N-6 and N-5 along with quinone functional groups on the doped carbons has shown significant effects on capacitive performance, which was proven by the high correlation coefficient (>0.99) between specific capacitance and the amounts of N-6, N-5, and quinone groups.[37a] A recent study has explored the detailed mechanisms regarding the redox reactions of nitrogen-containing functional groups through ex situ coupled XPS and CV study.[69] Two electrochemical redox reactions are proposed: 1) the redox reaction between N-5 (only pyridone-N) and N-6 and 2) the redox reaction between N-X and N-6. The reaction paths are shown in Figure 5a,b.[69] Since proton is involved in redox reactions for N-containing functional groups, the pseudocapacitance can be observed at less positive potentials when measured in acidic electrolytes.[64b] Although the alkaline solution lacks a proton, significant pseudocapacitance can still be achieved, probably due to the redox reactions involving ions such as potassium ion.[70] Compared with O-containing functional groups, the pseudocapacitance brought by N-containing functional groups is more stable, and less capacitance decay is obtained after cycling.[64a,71] However, N-containing functional groups show almost no benefits for pseudocapacitance in neutral electrolytes and nonaqueous electrolytes.[60b,70]

Although N doping on various forms of carbon materials has been widely investigated for EDLCs, the employment of N-

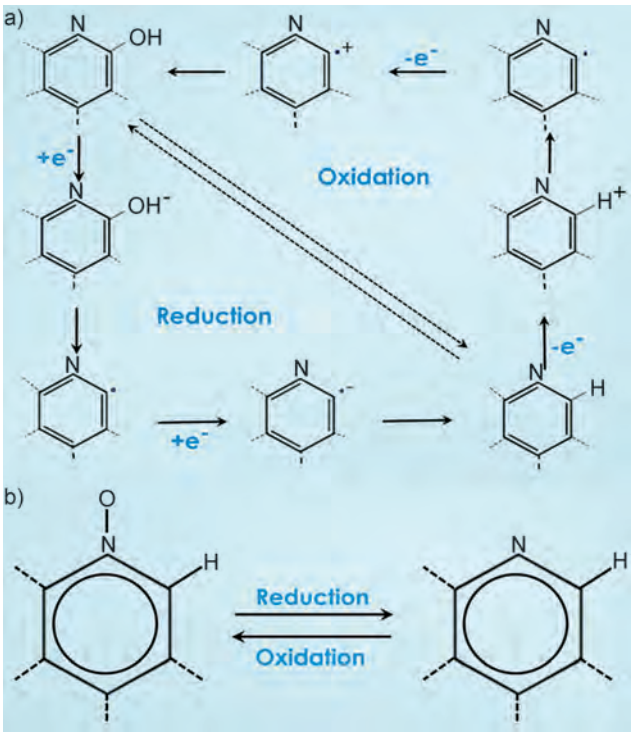

Figure 5. Reduction oxidation reactions in graphene. a) The reaction path between N-5 (pyridine N, upper left) and N-6 (lower right). b) The reaction path between N-X (left) and N-6 (right) (reprinted from reference [69] with permissions).

doped graphene as the electrode has been reported more recently.[37b,72] As indicated in previous study, N doping in conjunction with a relatively high specific surface area provides better capacitive performances compared to those of commercial ACs in both aqueous and nonaqueous electrolytes. The most representative example is the N-doped graphene demonstrated by Jeong et al.,[37b] in which excellent long-term stability, high power and energy capability, and compatibility with flexible substrates are shown, rendering N-doped graphene an extremely promising material for EDLCs. Other examples for N-doped graphene are summarized in Table 1.

4.3. Phosphorus doping and sulfur doping

The preparation of P-doped carbons usually involves the addition of phosphoric acid, which acts as either the activation agent for carbons[38a,73] or the P-containing molecules in the mixed precursors.[38b,74] Both lead to the formation of phosphate groups on the surface of graphene layers. Hulicova-Jurcakova et al.[75] introduced the incorporation of phosphorus to carbon materials for the first time through the study of N, P co-doping AC as the electrode material for EDLCs. The result indicates that the formation of surface pyrophosphates shows positive effects on the specific capacitance through redox reactions, whereas metaphosphates enhance the capacitance retention at high scan rates.[75] The increase of metaphosphates is also proposed to maintain the skeleton of the carbon structure by the creation of phosphate bridges.[73] On the other hand, since the structures of P–N and P=N are confirmed to enhance capacitive performances, the utilization of guanidine phosphate containing both nitrogen and phosphorus as precursors is reported, showing improved capacitive performance, although the higher pseudocapacitance contribution is ascribed to N doping in this case.[76] Although, like B doping, P doping easily brings in more O-containing functional groups and leads to faster decay of capacitance retention during a fast charge/discharge,[38a] P-doped carbons are actually more stable during cycling through the blockage of oxygen oxidation and hydrogen evolution due to the formation of a protective oxide layer on the surface.[40a,58] Hence, a wider potential window in H_2SO_4 extended to 1.5 V can be observed, resulting in the specific energy density of more than 13 W h kg^{-1}.[38a,74] P-doped graphene for EDLCs has not yet been reported, but improved capacitive performances provided by P doping establish the possibility to apply P-doped graphene in the near future.

S doping has been proposed to enhance the capacitive performances of EDLCs as well, but very few studies have been reported to date. G. Hasegawa et al.[39a] were the first to demonstrate S-doped carbons as an electrode material for EDLCs. The B doping can be achieved by the sulfonation of precursors prior to carbonization, which could suppress shrinkage of the carbon structure and maintain the mesopores and macropores in the structure.[39a,77] The incorporation of sulfur has been shown to increase the polarity on the carbon surface and reduce the charge-transfer resistance, leading to the improvement of capacitive performances.[39b] However, further investigations are needed to reveal the contribution of sulfur incorporation.

Table 1. Summary of the capacitive performance for N-doped graphene reported to date.

	Surface area [m^2 g^{-1}]	Electrolyte	N [%]	C_g [F g^{-1}]	C_{sa} [F m^{-2}]	SE[a] [Wh kg^{-1}]	SP[a] [W kg^{-1}]	Cyclic stability [cycles]	Ref.
1	466	1 M $HClO_4$	4.7 at% (N/C)	212.3	0.46	N/A	N/A	N/A	[108]
2	630.6	1 M Et_4NBF_4/PC	2 at%	138.1	0.22	76.7	1000	N/A	[72b]
3	N/A	6 M KOH	1.7–2.5 at%	282	N/A	N/A	N/A	230 000	[37b]
		1 M Et_4NBF_4		230	N/A	48	12 000	100 000	
4	346	0.5 M H_2SO_4	2–10 at% (N/C)	217.8	0.63	N/A	N/A	>1000	[61a]
5	N/A	6 M KOH	7.2 at%	144.6	N/A	N/A	N/A	500	[61b]
6	593	6 M KOH	10.1 at%	326	0.45	25	7980	2000	[61c]
7	465	1 M Bu_4NBF_4	10 wt%	248.4	0.53	N/A	N/A	5000	[109]
8	590	6 M KOH	1.2 at%	255	0.43	N/A	N/A	1200	[72a]

[a] Optimal values obtained from Ragone plots.

5. Electrode Materials Based on Graphene/ Metal Oxide Composites

Due to abundant defects and chemical moieties created during synthesis, the exceptional properties of graphene are greatly diminished. The intrinsic specific surface area of graphene composites is greatly reduced by aggregation and stacking between individual graphene sheets driven by the strong π–π interactions. In addition, as the intersheet contact resistance increases, the conductivity of graphene decreases. Previous studies on the capacitive behavior of graphene electrode materials indicate that the actual capacitive performance is much lower than the anticipated value estimated from the ultrahigh theoretical surface area because of the serious aggregation and restacking of graphene sheets resulting from strong van der Waals interactions between individual graphene sheets.[78] This phenomenon is the most serious issue when considering graphene for applications in various fields. Therefore, how to significantly inhibit the restacking and effectively expose the surface area of graphene sheets becomes an important topic in developing graphene-sheet-based electrode materials. Most researchers introduce extra additives during the preparation process, which may be a pure additive or an intrinsically active material for their applications. Accordingly, various graphene-based composites, including metal oxide nanoparticles/graphene sheet[79] and carbon nanomaterials/graphene sheet,[30] were demonstrated to solve the above restacking issue.

These hierarchical architectures of graphene-sheet-based composites (Figure 6a), including 1) superiorly conductive graphene sheets, 2) extra additives, and 3) macro-/mesospace, show some predominance as electrode materials. Here the extra additive, dispersed on the surface of graphene sheets, can act as a nanospacer to prevent the restacking of graphene sheets during the reduction of GO. On the other hand, superiorly conductive graphene with a length generally longer than 5 μm, which depends on the size of the graphene sheet, will provide a 2D smooth electronic superhighway for rapid charge storage and delivery. In addition, the high surface area graphene sheet also allows the uniform dispersion of extra additives to promote the utilization of electrode materials. Finally, the macro-/mesospace, constructed between the graphene sheet and nanoparticle, also facilitates the transport of electrolytes or reactants. Therefore, reservoirs for electrolytes or reactants can be formed within macro-/mesopores for facile transport of electrolytes or reactants in the short nanochannels. In addition, I. Honma et al. proposed that the space between graphene sheets and nanocrystallites can also be used as a flexible space for crystal expansion during the insertion of Li ions, significantly improving the poor cycle life of metal oxides.[80] Therefore, this design of hierarchical graphene-sheet-based composites considers not only issues of electrode materials, such as electron/electrolyte transport, utilization of electroactive species, and cycle life, but also the restacking of graphene sheets. Accordingly, novel graphene-sheet-based composites are very promising for next-generation high-performance electrode materials.

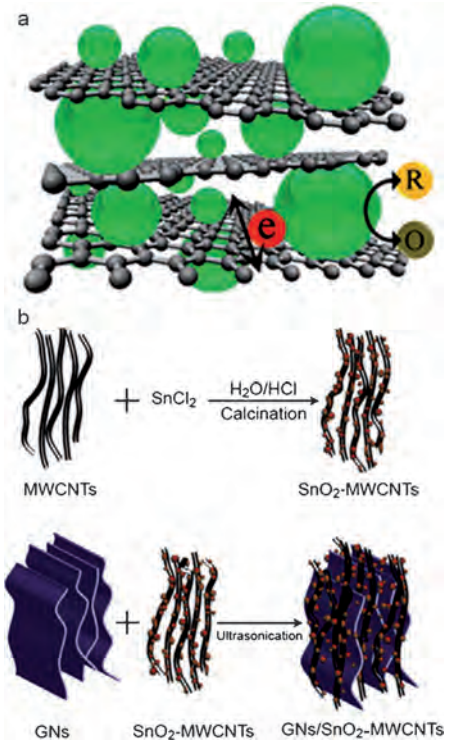

Figure 6. Graphene materials using spacers. a) A schematic illustration of hierarchical graphene-sheet-based composites, including superiorly conductive graphene sheets, nanospacers, and macro-/mesospaces. The nanospacer can be any metallic nanoparticle, oxide nanocrystallite, conductive polymer, or carbon nanomaterial. b) Schematic for the preparation of graphene/SnO_2-MWCNT composites (reproduced from reference [88] with permission).

L. Pan et al. reported graphene–ZnO and graphene–SnO_2 composites for supercapacitor applications.[81] Graphene–ZnO composites exhibit a higher capacitance of 61 $F g^{-1}$ with an energy density of 4.8 $W h kg^{-1}$, which was higher than that of graphene–SnO_2 samples. The results showed that the graphene–ZnO composite exhibited an improved electrochemical capacitance over that of pristine ZnO or pure graphene, with good reversible charge–discharge behavior.[81,82] In another article, Z. Fan et al. reported graphene/MnO_2 composites for supercapacitor applications.[83] The graphene/MnO_2 composite (at 78 wt% MnO_2) shows a specific capacitance of 310 $F g^{-1}$ at 2 $mV s^{-1}$. Thus, the hybridization of MnO_2 and graphene causes an increase in conductivity and specific surface area of the composites, ultimately leading to high rate performance.[83,84] Furthermore, our group proposed a novel two-step strategy to well-dispersed single-phase unitary and binary oxide nanocrystals (e.g., RuO_2, SnO_2, TiO_2, Mn_3O_4, $NiCo_2O_4$, and Zn_2SnO_4) onto graphene nanosheets for novel applications, including energy storage/conversion systems and sensors.[85] S. Ramaprabhu et al. also reported on graphene decoration with different metal oxides (such as RuO_2, TiO_2, and Fe_3O_4) as well as polyaniline by a chemical route.[86] The cyclic voltammetric studies at various sweep rates in 1 M H_2SO_4 show that RuO_2/graphene composites possess a higher specific capacitance of 220 $F g^{-1}$ at 10 $A g^{-1}$ than composites with other metal oxides, such as TiO_2 and Fe_3O_4. This is attributable to the better electrical con-

ductivity and reversible Faradic reactions of RuO_2 than those of other metal oxides. Similar results were obtained in another work by H. N. Alshareef et al.,[87] in which they reported various metal oxide composites (such as SnO_2, MnO_2, and RuO_2) with graphene nanosheets. Moreover, RuO_2/graphene (365 $F g^{-1}$) showed a higher specific capacitance than SnO_2/graphene (195 $F g^{-1}$). Furthermore, H. N. Alshareef et al.[88] reported on graphene nanosheet/SnO_2-MWCNT composites for supercapacitor applications (Figure 6b). The advantage of this structure is the significant inhibition of restacking and effective exposure of the surface area for graphene sheets. These nanocomposites achieved a high specific capacitance of 224 $F g^{-1}$, with an energy and power density of 31 $W h kg^{-1}$ and 17 $kW kg^{-1}$, respectively. The symmetric supercapacitor device fabricated using these nanocomposites shows 81% retention after 6000 cycles.

Q. Yan et al.[89] reported on a supercapacitor consisting of a Fe_3O_4/reduced graphene oxide (RGO) composite, which showed a specific capacitance of 480 $F g^{-1}$ at a discharge current density of 5 $A g^{-1}$; the corresponding energy and power densities were 67 $W h kg^{-1}$ and 5.5 $kW kg^{-1}$, respectively. C. M. Li et al. reported on CeO_2–graphene nanosheet composites, which show an improved specific capacitance of 208 $F g^{-1}$. This is due to a synergy effect contributing to the improved electronic conductivity of CeO_2 as well as to the better utilization of graphene.[90] Layered double hydroxides (LDHs, especially Co–Al) and graphene composites are a point of interest in some studies.[79,91] The studies show that the formation of LDHs prevents the restacking of graphene nanosheets; meanwhile, the formation of complex structures depends on the concentration of LDH ions. Furthermore, these studies reveal the advantages of these composites as a high specific surface area, more utilization of LDH structures, better conductivity, etc. These electrodes show a high specific capacitance of 1200 $F g^{-1}$ at a scan rate of 5 $mV s^{-1}$.[79] Our group[92] reported the microwave-assisted hydrothermal synthesis of Mn_3O_4/graphene composites for supercapacitor application. The aqueous asymmetric supercapacitor shows capacitor behavior with a cell voltage of up to 2 V, as shown in Figure 7a–d. These electrodes in the asymmetric configuration with nitrogen-doped graphene show energy and power densities of 11 $W h kg^{-1}$ and 24 $kW kg^{-1}$, respectively, at a current density of 24 $A g^{-1}$. This and some other results suggest that a graphene nanosheet could be used as an ideal conductive matrix for enhancing the capacitance performance of Mn_3O_4.[92,93]

P. Chen et al.[94] reported on the development of 3D porous graphene/cobalt oxide electrodes for a high-performance supercapacitor. These electrodes show high specific capacitance of 1100 $F g^{-1}$ at a current density of 10 $A g^{-1}$. T. Yu et al.[95] reported on the development of Co_3O_4/graphene composites for supercapacitor applications, which show a specific capacitance of 159 $F g^{-1}$ at a scan rate of 5 $mV s^{-1}$. In addition, cobalt oxide/graphene composites have been considered as one of the most promising materials for next-generation supercapacitors because of their advantages such as cost-effectiveness, environmental friendliness, and high specific capacitance.[96] X. S. Zhao et al.[97] reported on the development of a 3D nanostructure of nickel hydroxide/graphene composites for supercapacitor applications, in which nickel hydroxide embedded in a CNT acts as a pillar for graphene sheets. The supercapacitor study for this 3D nanostructure showed a high specific capacitance of 1235 $F g^{-1}$ at 1 $A g^{-1}$, but the capacitance decreased to 780 $F g^{-1}$ with an increase in current density (up to 20 $A g^{-1}$). The mass ratio of nickel to graphene, morphology, and microstructure were important to the performances of such nanocomposites.[98]

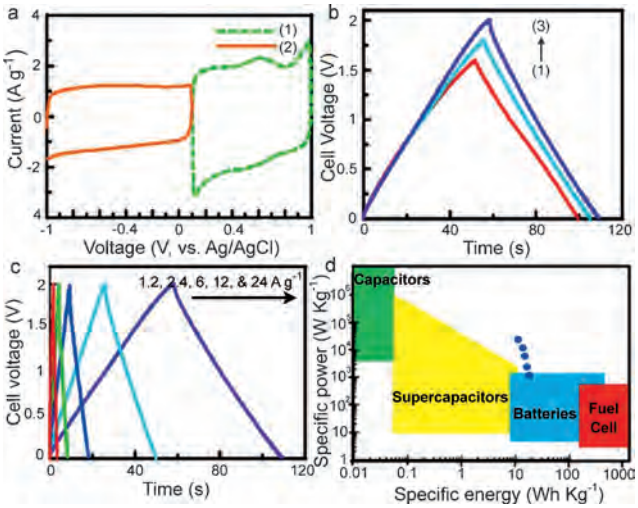

Figure 7. GO composites for supercapacitors. a) Cyclic voltammograms of (1) graphene-modified Mn_3O_4 and (2) N-doped RGO at 10 $mV s^{-1}$. b,c) The constant-current CD profiles of an asymmetric supercapacitor consisting of a graphene-modified Mn_3O_4 cathode and an N-doped RGO anode b) with the cell voltage of (1) 1.6, (2) 1.8, and (3) 2.0 V at 1.2 $A g^{-1}$ and c) with a cell voltage of 2.0 V at 1.2, 2.4, 6, 12, and 24 $A g^{-1}$. d) The Ragone plot for this asymmetric supercapacitor (reproduced from reference [92] with permission).

6. Electrode Materials Based on Graphene/Electrically Conducting Polymer Composites

Graphene/polymer composites have attracted great attention because of their high strength and improved conductivity. Graphene materials are often mixed with polymers to form composites, especially when fabricating flexible devices. There are several previous reports on the development of graphene/polymer composites as electrodes for different applications such as active layers of organic solar cells, counter electrodes of dye-sensitized solar cells, transparent conducting electrodes, catalytic electrodes, and polymer electrolyte membranes of fuel cells.[99] H. M. Cheng et al.[100a] reported on graphene/polyaniline composites by in situ anodic polymerization for flexible supercapacitors. These composites show a very good capacitance of 233 $F g^{-1}$ at a scan rate of 2 $mV s^{-1}$ and stability up to 1500 cycles. J. Xu et al.[100b] have reported the growth of polyaniline nanorod arrays on graphene sheets for supercapacitor applications (Figure 8a,b). These electrodes show a specific capacitance of 555 $F g^{-1}$ at a current density of 0.2 $A g^{-1}$ in 1 M H_2SO_4 solution and stability up to 2000 cycles. Recently, our group reported the development of layered graphene and polyaniline composites (TEM and SEM images are shown in

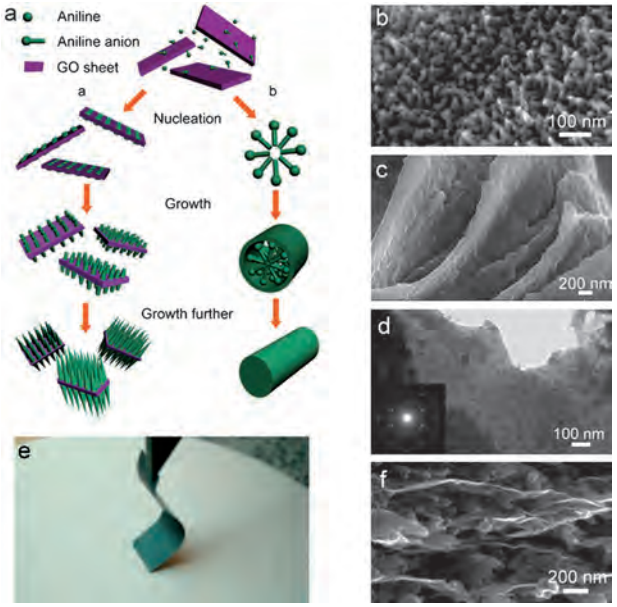

Figure 8. GO and conducting polymer composites. a) Schematic illustration of the nucleation and growth mechanism of PANI nanowires. b, c) SEM images of graphene oxide–polyaniline nanowire arrays (reproduced from reference [100b] with permission). d) TEM image of graphene oxide–polyaniline composites. The inset shows a SEAD pattern for the composites (reproduced from reference [23] with permission). e) Digital photograph of graphene–polyaniline nanofiber composite film. f) Cross-sectional SEM image of graphene–polyaniline nanofiber (reproduced from reference [101] with permission).

Figure 8c, d) for which we have obtained highest specific capacitance of 286 $F g^{-1}$ at a scan rate of 5 $mV s^{-1}$.[23] G. Shi et al.[101] reported a flexible supercapacitor based on flexible graphene and polyaniline nanofibers, which is shown in Figure 8e, f. The conductivity of polyaniline fibers was found to be increased up to 44% when the composite was made with graphene. This flexible supercapacitor shows a specific capacitance of 210 $F g^{-1}$ at a current density of 0.3 $A g^{-1}$. Many others reports involving graphene/polymer composites for supercapacitor applications are listed in Table 2.

As mentioned above, the π–π stacking between graphene sheets usually causes much lower real specific surface area than their theoretical values. In many cases, mixing with polymer increases the severity of this problem. There is need for development of new techniques for homogeneous mixing of single layered graphene sheets into polymer matrix. The construction of graphene-based 3D architectures in the composite form can overcome this problem.

7. Asymmetric Supercapacitors Based on Graphene Materials

The fabrication of asymmetric supercapacitors using aqueous electrolytes is an efficient way to improve the energy density of supercapacitors. The key to fabricating an asymmetric supercapacitor is to choose electrode materials with complementary working potential windows in the same electrolyte. In case of aqueous electrolyte, the main limitation is that the operating potential window cannot extended beyond their thermodynamic limit (1.23 V). However, by use of asymmetric supercapacitor configuration, we can easily bypass this problem by extending their operating potential window up to 2 V, which results in high-energy density supercapacitors.[102] For metal oxides and polymers, a limited potential window is a problem for the improvement of energy density; on the other hand, the small capacitance value of carbon material is also a limitation. The asymmetric configuration, however, could solve these problems.

Our group[103] reported on the development of an asymmetric cell consisting of a positive electrode of polyaniline nanofibers and a negative electrode of graphene nanosheets. The energy and power densities of this asymmetric supercapacitor consisting of PANI and graphene reach approximately 4.86 $W h kg^{-1}$ and 8.75 $kW kg^{-1}$, respectively, at 500 $mV s^{-1}$, which is promising in the application of next-generation supercapacitors. X. S. Zhao et al.[104] reported on the development of asymmetric supercapacitors based on graphene-modified ruthenium oxide (17% Ru) and graphene. The results showed an energy density of 26 $W h kg^{-1}$ at a power density of 49 $kW kg^{-1}$ for the configuration, which is more than double the symmetric configuration. The Ragone plots of symmetric and asymmetric supercapacitors based on RGO, RGO–RuO_2, and RGO–PANI are shown in Figure 9d. S. G. Lee et al.[105] reported a solid-state flexible asymmetric supercapacitor based on ionic-liquid-functionalized graphene and RuO_2. The comparative cyclic voltammograms (CVs) for both electrodes at a scan rate of 50 $mV s^{-1}$ (Figure 9a) and the asymmetric supercapacitor at different potential windows (Figure 9b) are shown. The galvanostatic charge–discharge curves for symmet-

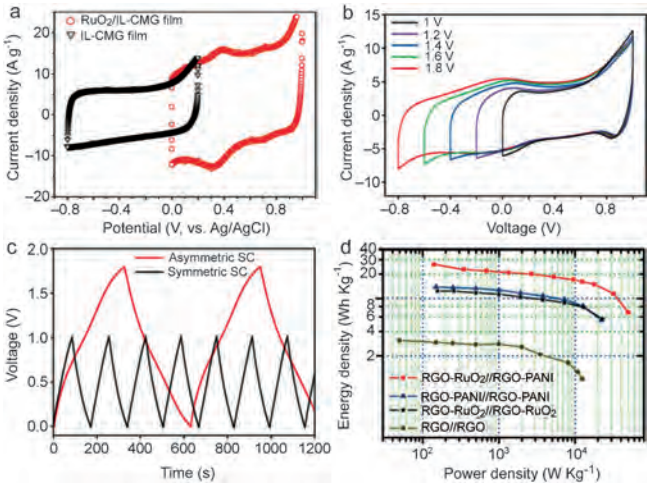

Figure 9. Asymmetric supercapacitors based on GO. a) Comparative CV curves obtained for chemically modified graphene and RuO_2 chemically modified graphene films in aqueous 1 M H_2SO_4 solution at a scan rate of 50 $mV s^{-1}$ (reproduced from reference [105] with permission). b) CV curves obtained from asymmetric SC devices with different cell voltages of 1, 1.2, 1.4, 1.6, and 1.8 V at a scan rate of 50 $mV s^{-1}$ (reproduced from reference [105] with permission). c) Galvanostatic charge–discharge studies of symmetric and asymmetric supercapacitor. d) Ragone plots of symmetric and asymmetric supercapacitors based on RGO, RGO–RuO_2, and RGO–PANI (reproduced from reference [104] with permission).

Table 2. The electrode material, electrolytes and electrochemical parameters used for different graphene–polymer nanocomposites.[a]

Electrode materials	Electrolyte ([mol L^{-1}])	C [F g^{-1}]	Current density	Scan rate [mV s^{-1}]	Cycles	Ref.
Ppy-decorated G	$NaNO_3$ (1)	294	10 mA cm^{-2}	–	–	[110]
P–PANI–G	$HClO_4$ (1)	878	1 A g^{-1}	–	1000	[111]
CFGO–PANI	H_2SO_4 (1)	525	0.3 A g^{-1}	–	200	[112]
G–Ppy nanotubes	H_2SO_4 (2)	400	0.3 A g^{-1}	–	200	[113]
Ppy–GNP	Na_2SO_4 (0.5)	285	0.5 A g^{-1}	–	1000	[114]
G–PANI	H_2SO_4 (2)	526	0.2 A g^{-1}	–	–	[115]
PANI–RGO	H_2SO_4 (1)	250	–	10	–	[116]
G–Ppy	H_2SO_4 (2)	417	–	10	500	[117]
G–Ppy	$LiClO_4$ (0.1)	1510	–	10	–	[118]
GO–PANI	H_2SO_4 (1)	489	400 mA g^{-1}	–	500	[119]
G–PANI	H_2SO_4 (1)	1126	–	1	1000	[120]
GNS–Ppy	NaCl (1)	165	1 A g^{-1}	–	1000	[121]
GO–PANI	H_2SO_4 (1)	746	200 mA g^{-1}	–	500	[122]
PNW–GOS	H_2SO_4 (1)	555	0.2 A g^{-1}	–	2000	[100b]
G–PANI	H_2SO_4 (2)	480	0.1 A g^{-1}	–	1000	[123]
PpPD–G	H_2SO_4 (1)	248	2 A g^{-1}	–	1000	[124]
GNS–PANI	H_2SO_4 (1)	375	0.5 A g^{-1}	–	500	[7b]
G–Ppy	H_2SO_4 (1)	335	1 A g^{-1}	–	1000	[125]
G–Ppy	H_2SO_4 (1)	420	0.5 A g^{-1}	–	200	[126]
G–PANI	$Et_4N^+ \cdot BF_4^-$/PC (1)	250	0.5 A g^{-1}	–	1000	[127]
G–PANI	H_2SO_4 (1)	346	4 A g^{-1}	–	600	[128]
G–CP	H_2SO_4 (1)	201	–	10	100	[129]
RGO–PANI	H_2SO_4 (0.5)	970	2.5 A g^{-1}	–	1700	[130]
GO–Ppy	KCl (0.1)	356	0.5 A g^{-1}	–	1000	[131]
G–PEDOT	H_2SO_4 (2)	342	20 mA cm^{-2}	–	–	[132]
GNS–PANI	H_2SO_4 (1)	1130	–	5	1000	[133]
G–Ppy	KCl (1)	237	–	100	–	[134]
G–Ppy	H_2SO_4 (1)	318	–	2	1000	[135]
G–PANI	H_2SO_4 (1)	640	0.1 A g^{-1}	–	1000	[136]
GO–Ppy	H_2SO_4 (1)	510	0.3 A g^{-1}	–	1000	[137]
G-doped PANI	H_2SO_4 (1)	531	200 mA g^{-1}	–	–	[138]
G–PANI	H_2SO_4 (1)	233	–	2	1500	[100a]
G–PANI	H_2SO_4 (1)	210	0.3 A g^{-1}	–	800	[101]

[a] Ppy: polypyrrole; G: graphene; PANI: polyaniline; CFGO: carboxyl-functionalized graphene oxide; GNP: graphene nanoplatelates; PNW: polyanilyne nanowires; GOS: graphene oxide sheets; PC: propylene carbonate; CP: poly(3,4-propylenedioxythiophene); PEDOT: polyethylenedioxythiophene.

ric and asymmetric supercapacitor are shown in Figure 9c. This asymmetric supercapacitor shows energy and power densities of 19.7 W h kg^{-1} and 0.5 kW kg^{-1}, respectively, for a current density of 0.5 A g^{-1}. An asymmetric supercapacitor based on graphene hydrogel and MnO_2 nanoflakes on nickel foam was reported by H. Duan et al.[106] This asymmetric supercapacitor can be cycled reversibly in a wide voltage window from 0 to 2 V and exhibits an energy density of 23 W h kg^{-1} with a power density of 1.0 kW kg^{-1}. Thus, graphene has been shown to be an important material in the asymmetric combination when widening the cell voltage to 2 V for metal oxides and also useful for future solid-state devices based on a polymer gel electrolyte.[107]

8. Summary and Outlook

Graphene is a very attractive electrode material for energy storage. We can find many advantages, such as high specific surface area, an interconnected porous structure, a controlled pore size that matches electrolyte ions, good wettability toward the electrolyte, and high electrical conductivity. Although pristine graphene has a significantly lower capacitance value than we expected, improved energy storage performance can be achieved by combining double-layer capacitance together with fast and highly reversible pseudocapacitance. For example, the synthesis of graphene-based composites, the use of ionic liquids with an electrochemically stable window of 4 V, and the fabrication of asymmetric configurations (e.g., a positive electrode of Mn_3O_4/graphene composites and a negative electrode of N-doped graphene sheets) can maximize the working potential range for each electrode, resulting in a wide potential window. A higher cell voltage improves both energy and power densities, as it is proportional to the voltage window (V^2). The safe operation with 'green chemistry' is a promising electrochemical system for the next generation of supercapacitor applications. For the next generation of graphene-based supercapacitors, it is expected that energy, power, and reliability, which are required for modern technology, will increase. In the future, the challenging issue in supercapacitor fields will be the development of highly efficient materials through cost-effective methods in order to realize their excellent performance, which is not attainable by other energy storage devices. Thus, future research should be directed toward the development of electrode materials with a high charge capacity and minimum ESR.

Keywords: carbon · energy storage · graphene · nanostructures · porous materials

[1] a) H. Jiang, P. S. Lee, C. Z. Li, *Energy Environ. Sci.* **2013**, *6*, 41–53; b) J. Zhang, X. S. Zhao, *ChemSusChem* **2012**, *5*, 818–841; c) S. Bose, T. Kuila, A. K. Mishra, R. Rajasekar, N. H. Kim, J. H. Lee, *J. Mater. Chem.* **2012**, *22*, 767–784; d) M. Winter, R. J. Brodd, *Chem. Rev.* **2004**, *104*, 4245–4269; e) A. Burke, *J. Power Sources* **2000**, *91*, 37–50.

[2] P. Simon, Y. Gogotsi, *Nat. Mater.* **2008**, *7*, 845–854.

[3] B. E. Conway, *Electrochemical Supercapacitors: Scientific Fundamentals and Technological Applications*, Kluwer Academic/Plenum Publisher, New York, **1999**.

[4] a) N. L. Torad, M. Hu, Y. Kamachi, K. Takai, M. Imura, M. Naito, Y. Yamauchi, *Chem. Commun.* **2013**, *49*, 2521–2523; b) M. Hu, J. Reboul, S. Furukawa, N. L. Torad, Q. Ji, P. Srinivasu, K. Ariga, S. Kitagawa, Y. Yamauchi, J. *Am. Chem. Soc.* **2012**, *134*, 2864–2867; c) W. Chaikittisilp, K. Ariga, Y. Yamauchi, *J. Mater. Chem. A* **2013**, *1*, 14; d) L. Radhakrishnan, J. Reboul, S. Furukawa, P. Srinivasu, S. Kitagawa, Y. Yamauchi, *Chem. Mater.* **2011**, *23*, 1225–1231.

[5] a) W. Chaikittisilp, M. Hu, H. Wang, H. S. Huang, T. Fujita, K. C. Wu, L. C. Chen, Y. Yamauchi, K. Ariga, *Chem. Commun.* **2012**, *48*, 7259–7261; b) N. L. Torad, R. R. Salunkhe, Y. Li, H. Hamoudi, M. Imura, Y. Sakka, C. C. Hu, Y. Yamauchi, *Chem. Eur. J.* **2014**, 20, 7895–7900.

[6] a) C. C. Hu, J. Y. Lin, *Electrochim. Acta* **2002**, *47*, 4055–4067; b) C. C. Hu, X. X. Lin, *J. Electrochem. Soc.* **2002**, *149*, A1049–A1057.

[7] a) H. Y. Hsu, K. H. Chang, R. R. Salunkhe, C. T. Hsu, C. C. Hu, *Electrochim. Acta* **2013**, *94*, 104–112; b) R. R. Salunkhe, K. Jang, S. W. Lee, H. Ahn, *RSC Adv.* **2012**, *2*, 3190–3193; c) R. R. Salunkhe, K. Jang, H. Yu, S. Yu, T. Ganesh, S. H. Han, H. Ahn, *J. Alloys Compd.* **2011**, *509*, 6677–6682.

[8] a) D. S. Dhawale, D. P. Dubal, V. S. Jamadade, R. R. Salunkhe, C. D. Lokhande, *Synth. Met.* **2010**, *160*, 519 – 522; b) C. C. Hu, C. H. Chu, *Mater. Chem. Phys.* **2000**, *65*, 329 – 338.

[9] a) K. H. Chang, C. C. Hu, *Appl. Phys. Lett.* **2006**, *88*, 193102; b) C. C. Hu, K. H. Chang, M. C. Lin, Y. T. Wu, *Nano Lett.* **2006**, *6*, 2690 – 2695; c) K. M. Lin, K. H. Chang, C. C. Hu, Y. Y. Li, *Electrochim. Acta* **2009**, *54*, 4574 – 4581; d) W. Sugimoto, S. Makino, R. Mukai, Y. Tatsumi, K. Fukuda, Y. Takasu, Y. Yamauchi, *J. Power Sources* **2012**, *204*, 244 – 248; e) S. Makino, Y. Yamauchi, W. Sugimoto, *J. Power Sources* **2013**, *227*, 153 – 160; f) H. S. Huang, K. H. Chang, N. Suzuki, Y. Yamauchi, C. C. Hu, K. C. Wu, *Small* **2013**, *9*, 2520 – 2526; g) B. P. Bastakoti, H. Oveisi, C. C. Hu, K. C. W. Wu, N. Suzuki, K. Takai, Y. Kamachi, M. Imura, Y. Yamauchi, *Eur. J. Inorg. Chem.* **2013**, 1109 – 1112; h) M. Hu, S. Ishihara, Y. Yamauchi, *Angew. Chem.* **2013**, *125*, 1273 – 1277; *Angew. Chem. Int. Ed.* **2013**, *52*, 1235 – 1239; i) B. P. Bastakoti, R. R. Salunkhe, J. Ye, Y. Yamauchi, *Phys. Chem. Chem. Phys.* **2014**, *16*, 10425 – 10428.

[10] a) B. P. Bastakoti, H. S. Huang, L. C. Chen, K. C. Wu, Y. Yamauchi, *Chem. Commun.* **2012**, *48*, 9150 – 9152; b) B. P. Bastakoti, Y. Kamachi, H. S. Huang, L. C. Chen, K. C. W. Wu, Y. Yamauchi, *Eur. J. Inorg. Chem.* **2013**, 39 – 43; c) R. R. Salunkhe, B. P. Bastakoti, C. T. Hsu, N. Suzuki, J. H. Kim, S. X. Dou, C. C. Hu, Y. Yamauchi, *Chem. Eur. J.* **2014**, *20*, 3084 – 3088.

[11] a) G. X. Zhao, T. Wen, C. L. Chen, X. K. Wang, *RSC Adv.* **2012**, *2*, 9286 – 9303; b) B. Luo, S. Liu, L. Zhi, *Small* **2012**, *8*, 630 – 646; c) Y. Huang, J. Liang, Y. Chen, *Small* **2012**, *8*, 1805 – 1834; d) H. J. Choi, S. M. Jung, J. M. Seo, D. W. Chang, L. Dai, J. B. Baek, *Nano Energy* **2012**, *1*, 534 – 551.

[12] a) A. K. Geim, K. S. Novoselov, *Nat. Mater.* **2007**, *6*, 183 – 191; b) C. N. Rao, A. K. Sood, K. S. Subrahmanyam, A. Govindaraj, *Angew. Chem.* **2009**, *121*, 7890 – 7916; *Angew. Chem. Int. Ed.* **2009**, *48*, 7752 – 7777.

[13] D. A. Brownson, D. K. Kampouris, C. E. Banks, *Chem. Soc. Rev.* **2012**, *41*, 6944 – 6976.

[14] D. R. Dreyer, S. Park, C. W. Bielawski, R. S. Ruoff, *Chem. Soc. Rev.* **2010**, *39*, 228 – 240.

[15] a) L. L. Zhang, R. Zhou, X. S. Zhao, *J. Mater. Chem.* **2010**, *20*, 5983 – 5992.

[16] M. D. Stoller, S. J. Park, Y. W. Zhu, J. H. An, R. S. Ruoff, *Nano Lett.* **2008**, *8*, 3498 – 3502.

[17] S. R. C. Vivekchand, C. S. Rout, K. S. Subrahmanyam, A. Govindaraj, C. N. R. Rao, *J. Chem. Sci.* **2008**, *120*, 9 – 13.

[18] Q. Du, M. Zheng, L. Zhang, Y. Wang, J. Chen, L. Xue, W. Dai, G. Ji, J. Cao, *Electrochim. Acta* **2010**, *55*, 3897 – 3903.

[19] S. H. Lee, H. W. Kim, J. O. Hwang, W. J. Lee, J. Kwon, C. W. Bielawski, R. S. Ruoff, S. O. Kim, *Angew. Chem.* **2010**, *122*, 10282 – 10286; *Angew. Chem. Int. Ed.* **2010**, *49*, 10084 – 10088.

[20] C. Liu, Z. Yu, D. Neff, A. Zhamu, B. Z. Jang, *Nano Lett.* **2010**, *10*, 4863 – 4868.

[21] X. Cao, Y. Shi, W. Shi, G. Lu, X. Huang, Q. Yan, Q. Zhang, H. Zhang, *Small* **2011**, *7*, 3163 – 3168.

[22] Z. Xu, Z. Li, C. M. B. Holt, X. Tan, H. Wang, B. S. Amirkhiz, T. Stephenson, D. Mitlin, *J. Phys. Chem. Lett.* **2012**, *3*, 2928 – 2933.

[23] R. R. Salunkhe, S. H. Hsu, K. C. Wu, Y. Yamauchi, *ChemSusChem* **2014**, *7*, 1551 – 1556.

[24] K. S. Kim, S. J. Park, *Electrochim. Acta* **2011**, *56*, 1629 – 1635.

[25] G. Ning, Z. Fan, G. Wang, J. Gao, W. Qian, F. Wei, *Chem. Commun.* **2011**, *47*, 5976 – 5978.

[26] Y. X. Xu, K. X. Sheng, C. Li, G. Q. Shi, *ACS Nano* **2010**, *4*, 4324 – 4330.

[27] M. M. Hantel, T. Kaspar, R. Nesper, A. Wokaun, R. Kötz, *Electrochem. Commun.* **2011**, *13*, 90 – 92.

[28] Z. B. Lei, N. Christov, X. S. Zhao, *Energy Environ. Sci.* **2011**, *4*, 1866 – 1873.

[29] Y. S. Wang, S. Y. Yang, S. M. Li, H. W. Tien, S. T. Hsiao, W. H. Liao, C. H. Liu, K. H. Chang, C. C. M. Ma, C. C. Hu, *Electrochim. Acta* **2013**, *87*, 261 – 269.

[30] Y. Wang, Y. Wu, Y. Huang, F. Zhang, X. Yang, Y. Ma, Y. Chen, *J. Phys. Chem. C* **2011**, *115*, 23192 – 23197.

[31] S. Y. Yang, K. H. Chang, Y. F. Lee, C. C. M. Ma, C. C. Hu, *Electrochem. Commun.* **2010**, *12*, 1206 – 1209.

[32] J. J. Yoo, K. Balakrishnan, J. Huang, V. Meunier, B. G. Sumpter, A. Srivastava, M. Conway, A. L. Reddy, J. Yu, R. Vajtai, P. M. Ajayan, *Nano Lett.* **2011**, *11*, 1423 – 1427.

[33] F. C. Wu, R. L. Tseng, C. C. Hu, C. C. Wang, *J. Power Sources* **2006**, *159*, 1532 – 1542.

[34] Y. Li, M. van Zijll, S. Chiang, N. Pan, *J. Power Sources* **2011**, *196*, 6003 – 6006.

[35] Y. Zhu, S. Murali, M. D. Stoller, K. J. Ganesh, W. Cai, P. J. Ferreira, A. Pirkle, R. M. Wallace, K. A. Cychosz, M. Thommes, D. Su, E. A. Stach, R. S. Ruoff, *Science* **2011**, *332*, 1537 – 1541.

[36] a) S. Shiraishi, M. Kibe, T. Yokoyama, H. Kurihara, N. Patel, A. Oya, Y. Kaburagi, Y. Hishiyama, *Appl. Phys. A* **2006**, *82*, 585 – 591; b) D. W. Wang, F. Li, Z. G. Chen, G. Q. Lu, H. M. Cheng, *Chem. Mater.* **2008**, *20*, 7195 – 7200.

[37] a) D. Hulicova-Jurcakova, M. Seredych, G. Q. Lu, T. J. Bandosz, *Adv. Funct. Mater.* **2009**, *19*, 438 – 447; b) H. M. Jeong, J. W. Lee, W. H. Shin, Y. J. Choi, H. J. Shin, J. K. Kang, J. W. Choi, *Nano Lett.* **2011**, *11*, 2472 – 2477.

[38] a) D. Hulicova-Jurcakova, A. M. Puziy, O. I. Poddubnaya, F. S. Garcia, J. M. Tascon, G. Q. Lu, *J. Am. Chem. Soc.* **2009**, *131*, 5026 – 5027; b) X. C. Zhao, A. Q. Wang, J. W. Yan, G. Q. Sun, L. X. Sun, T. Zhang, *Chem. Mater.* **2010**, *22*, 5463 – 5473.

[39] a) G. Hasegawa, M. Aoki, K. Kanamori, K. Nakanishi, T. Hanada, K. Tadanaga, *J. Mater. Chem.* **2011**, *21*, 2060 – 2063; b) X. Zhao, Q. Zhang, C.-M. Chen, B. Zhang, S. Reiche, A. Wang, T. Zhang, R. Schlögl, D. Sheng Su, *Nano Energy* **2012**, *1*, 624 – 630.

[40] a) B. F. Abramovic, L. J. Bjelica, F. F. Gaal, V. J. Guzsvany, L. S. Jovanovic, *Electroanalysis* **2003**, *15*, 878 – 884; b) H. L. Guo, Q. M. Gao, *J. Power Sources* **2009**, *186*, 551 – 556; c) H. Konno, T. Ito, M. Ushiro, K. Fushimi, K. Azumi, *J. Power Sources* **2010**, *195*, 1739 – 1746.

[41] J. P. Randin, E. Yeager, *J. Electroanal. Chem.* **1974**, *54*, 93 – 100.

[42] C. Morena-Castilla, M. B. Dawidziuk, F. C. Marin, Z. Z. Benabithe, *Carbon* **2011**, *49*, 3808 – 3819.

[43] X. L. Zhai, Y. Song, J. Q. Liu, P. Li, M. Zhong, C. Ma, H. Q. Wang, Q. G. Guo, L. J. Zhi, *J. Electrochem. Soc.* **2012**, *159*, E177 – E182.

[44] H. Konno, T. Nakahashi, M. Inagaki, T. Sogabe, *Carbon* **1999**, *37*, 471 – 475.

[45] T. Tomko, R. Rajagopalan, P. Aksoy, H. C. Foley, *Electrochim. Acta* **2011**, *56*, 5369 – 5375.

[46] H. Gerischer, *J. Phys. Chem.* **1985**, *89*, 4249 – 4251.

[47] O. Barbieri, M. Hahn, A. Herzog, R. Kotz, *Carbon* **2005**, *43*, 1303 – 1310.

[48] M. Hahn, M. Baertschi, O. Barbieri, J. C. Sauter, R. Kotz, R. Gallay, *Electrochem. Solid-State Lett.* **2004**, *7*, A33 – A36.

[49] P. N. Vishwakarma, S. V. Subramanyam, *J. Appl. Phys.* **2006**, *100*, 113702.

[50] T. Liao, C. H. Sun, A. J. Du, Z. Q. Sun, D. H. Jurcakova, S. Smith, *J. Mater. Chem.* **2012**, *22*, 8321 – 8326.

[51] T. Liao, C. H. Sun, Z. Q. Sun, A. J. Du, D. H. Jurcakova, S. C. Smith, *J. Mater. Chem.* **2012**, *22*, 13751 – 13755.

[52] D. H. Zhong, H. Sano, Y. Uchiyama, K. Kobayashi, *Carbon* **2000**, *38*, 1199 – 1206.

[53] L. R. Radovic, M. Karra, K. Skokova, P. A. Thrower, *Carbon* **1998**, *36*, 1841 – 1854.

[54] X. X. Wu, L. R. Radovic, *J. Phys. Chem. A* **2004**, *108*, 9180 – 9187.

[55] T. Kwon, H. Nishihara, H. Itoi, Q. H. Yang, T. Kyotani, *Langmuir* **2009**, *25*, 11961 – 11968.

[56] L. S. Panchokarla, K. S. Subrahmanyam, S. K. Saha, A. Govindaraj, H. R. Krishnamurthy, U. V. Waghmare, C. N. R. Rao, *Adv. Mater.* **2009**, *21*, 4726 – 4730.

[57] Z. S. Wu, W. C. Ren, L. Xu, F. Li, H. M. Cheng, *ACS Nano* **2011**, *5*, 5463 – 5471.

[58] a) T. Durkic, A. Peric, M. Lausevic, A. Dekanski, O. Neskovic, M. Veljkovic, Z. Lausevic, *Carbon* **1997**, *35*, 1567 – 1572; b) M. B. Wu, Y. Y. Ren, N. Guo, S. B. Li, X. Y. Sun, M. H. Tan, D. Wang, J. T. Zheng, N. Tsubaki, *Mater. Lett.* **2012**, *82*, 124 – 126.

[59] a) K. Jurewicz, K. Babeł, R. Pietrzak, S. Delpeux, H. Wachowska, *Carbon* **2006**, *44*, 2368 – 2375; b) K. Jurewicz, K. Babeł, A. Źiółkowski, H. Wachowska, *Electrochim. Acta* **2003**, *48*, 1491 – 1498; c) N. D. Kim, W. Kim, J. B. Joo, S. Oh, P. Kim, Y. Kim, J. Yi, *J. Power Sources* **2008**, *180*, 671 –675.

[60] a) Y. J. Kim, Y. Abe, T. Yanagiura, K. C. Park, M. Shimizu, T. Iwazaki, S. Nakagawa, M. Endo, M. S. Dresselhaus, *Carbon* **2007**, *45*, 2116 – 2125; b) D. Hulicova, J. Yamashita, Y. Soneda, H. Hatori, M. Kodama, *Chem. Mater.* **2005**, *17*, 1241 – 1247.

[61] a) L. F. Lai, L. W. Chen, D. Zhan, L. Sun, J. P. Liu, S. H. Lim, C. K. Poh, Z. X. Shen, J. Y. Lin, *Carbon* **2011**, *49*, 3250 – 3257; b) B. J. Jiang, C. G. Tian, L. Wang, L. Sun, C. Chen, X. Z. Nong, Y. J. Qiao, H. G. Fu, *Appl. Surf. Sci.* **2012**, *258*, 3438 – 3443; c) L. Sun, L. Wang, C. Tian, T. Tan, Y. Xie, K. Shi, M. Li, H. Fu, *RSC Adv.* **2012**, *2*, 4498 – 4506.

[62] Y. Shao, S. Zhang, M. H. Engelhard, G. Li, G. Shao, Y. Wang, J. Liu, I. A. Aksay, Y. Lin, *J. Mater. Chem.* **2010**, *20*, 7491 – 7496.

[63] a) T. E. Rufford, D. Hulicova-Jurcakova, Z. Zhu, G. Q. Lu, *Electrochem. Commun.* **2008**, *10*, 1594 – 1597; b) M. Seredych, D. Hulicova-Jurcakova, G. Q. Lu, T. J. Bandosz, *Carbon* **2008**, *46*, 1475 – 1488.

[64] a) E. Frackowiak, G. Lota, J. Machnikowski, C. Vix-Guterl, F. Beguin, *Electrochim. Acta* **2006**, *51*, 2209 – 2214; b) Y. H. Lee, K. H. Chang, C. C. Hu, *J. Power Sources* **2013**, *227*, 300 – 308; c) C. Vagner, G. Finqueneisel, T. Zimny, P. Burg, B. Grzyb, J. Machnikowski, J. V. Weber, *Carbon* **2003**, *41*, 2847 – 2853; d) Y. R. Nian, H. S. Teng, *J. Electrochem. Soc.* **2002**, *149*, A1008 – A1014; e) D. W. Wang, F. Li, M. Liu, H. M. Cheng, *New Carbon Mater.* **2007**, *22*, 307 – 314; f) R. L. Mccreery, K. K. Cline, C. A. Mcdermott, M. T. Mcdermott, *Coll. Surf. A* **1994**, *93*, 211 – 219.

[65] M. J. Bleda-Martínez, J. A. M. Agulló, D. L. Castelló, E. Morallón, D. C. Amorós, A. L. Solano, *Carbon* **2005**, *43*, 2677 – 2684.

[66] G. Lota, K. Lota, E. Frackowiak, *Electrochem. Commun.* **2007**, *9*, 1828 – 1832.

[67] N. E. Derradji, M. L. Mahdjoubi, H. Belkhir, N. Mumumbila, B. Angleraud, F. Tessier, *Thin Solid Films* **2005**, *482*, 258 – 263.

[68] a) D. Hulicova Jurcakova, M. Kodama, S. Shiraishi, H. Hatori, Z. H. Zhu, G. Q. Lu, *Adv. Funct. Mater.* **2009**, *19*, 1800 – 1809; b) E. Frackowiak, *Phys. Chem. Chem. Phys.* **2007**, *9*, 1774.

[69] D. W. Wang, F. Li, L. C. Yin, X. Lu, Z. G. Chen, I. R. Gentle, G. Q. M. Lu, H. M. Cheng, *Chem. Eur. J.* **2012**, *18*, 5345 – 5351.

[70] a) D. Hulicova, M. Kodama, H. Hatori, *Chem. Mater.* **2006**, *18*, 2318 – 2326; b) G. Lota, E. Frackowiak, *Fuel Cells* **2010**, *10*, 848 – 855.

[71] a) C. O. Ania, V. Khomenko, E. Raymundo-Pinero, J. B. Parra, F. Beguin, *Adv. Funct. Mater.* **2007**, *17*, 1828 – 1836; b) G. Lota, B. Grzyb, H. Machnikowska, J. Machnikowski, E. Frackowiak, *Chem. Phys. Lett.* **2005**, *404*, 53 – 58.

[72] a) Z. B. Lei, L. Lu, X. S. Zhao, *Energy Environ. Sci.* **2012**, *5*, 6391 – 6399; b) Y. C. Qiu, X. F. Zhang, S. H. Yang, *Phys. Chem. Chem. Phys.* **2011**, *13*, 12554 – 12558.

[73] A. Castro-Muñiz, F. Suarez-Garcia, A. M. Alonso, J. M. D. Tascon, *J. Colloid Interface Sci.* **2011**, *361*, 307 – 315.

[74] D. Carriazo, M. C. Gutierrez, F. Pico, J. M. Rojo, J. L. G. Fierro, M. L. Ferrer, F. D. Monte, *ChemSusChem* **2012**, *5*, 1405 – 1409.

[75] D. Hulicova-Jurcakova, M. Seredych, G. Q. Lu, N. K. A. C. Kodiweera, P. E. Stallworth, S. Greenbaum, T. J. Bandosz, *Carbon* **2009**, *47*, 1576 – 1584.

[76] T. Tsubota, Y. Miyauchi, N. Murakami, T. Ohno, *J. Power Sources* **2011**, *196*, 5769 – 5773.

[77] G. Hasegawa, K. Kanamori, K. Nakanishi, T. Hanada, *Carbon* **2010**, *48*, 1757 – 1766.

[78] F. Zhang, J. Tang, N. Shinya, L. C. Qin, *Chem. Phys. Lett.* **2013**, *584*, 124 – 129.

[79] X. Dong, L. Wang, D. Wang, C. Li, J. Jin, *Langmuir* **2012**, *28*, 293 – 298.

[80] E. Yoo, J. Kim, E. Hosono, H. Zhou, T. Kudo, I. Honma, *Nano Lett.* **2008**, *8*, 2277 – 2282.

[81] T. Lu, Y. Zhang, H. Li, L. Pan, Y. Li, Z. Sun, *Electrochim. Acta* **2010**, *55*, 4170 – 4173.

[82] a) T. Lu, L. Pan, H. Li, G. Zhu, T. Lv, X. Liu, Z. Sun, T. Chen, D. H. C. Chua, *J. Alloys Compd.* **2011**, *509*, 5488 – 5492; b) J. Wang, Z. Gao, Z. Li, B. Wang, Y. Yan, Q. Liu, T. Mann, M. Zhang, Z. Jiang, *J. Solid State Chem.* **2011**, *184*, 1421 – 1427.

[83] J. Yan, Z. Fan, T. Wei, W. Qian, M. Zhang, F. Wei, *Carbon* **2010**, *48*, 3825 – 3833.

[84] a) Q. Cheng, J. Tang, J. Ma, H. Zhang, N. Shinya, L. C. Qin, *Carbon* **2011**, *49*, 2917 – 2925; b) Z. P. Li, Y. J. Mi, X. H. Liu, S. Liu, S. R. Yang, J. Q. Wang, *J. Mater. Chem.* **2011**, *21*, 14706 – 14711; c) M. Sathish, S. Mitani, T. Tomai, I. Honma, *J. Mater. Chem.* **2011**, *21*, 16216 – 16222; d) G. Yu, L. Hu, N. Liu, H. Wang, M. Vosgueritchian, Y. Yang, Y. Cui, Z. Bao, *Nano Lett.* **2011**, *11*, 4438 – 4442; e) L. Mao, K. Zhang, H. S. O. Chan, J. S. Wu, *J. Mater. Chem.* **2012**, *22*, 1845 – 1851.

[85] K. H. Chang, Y. F. Lee, C. C. Hu, C. I. Chang, C. L. Liu, Y. L. Yang, *Chem. Commun.* **2010**, *46*, 7957 – 7959.

[86] A. K. Mishra, S. Ramaprabhu, *J. Phys. Chem. C* **2011**, *115*, 14006 – 14013.

[87] R. B. Rakhi, W. Chen, D. Cha, H. N. Alshareef, *J. Mater. Chem.* **2011**, *21*, 16197 – 16204.

[88] R. B. Rakhi, H. N. Alshareef, *J. Power Sources* **2011**, *196*, 8858 – 8865.

[89] W. Shi, J. Zhu, D. H. Sim, Y. Y. Tay, Z. Lu, X. Zhang, Y. Sharma, M. Srinivasan, H. Zhang, H. H. Hng, Q. Yan, *J. Mater. Chem.* **2011**, *21*, 3422.

[90] Y. Wang, C. X. Guo, J. Liu, T. Chen, H. Yang, C. M. Li, *Dalton Trans.* **2011**, *40*, 6388 – 6391.

[91] a) S. Huang, G. N. Zhu, C. Zhang, W. W. Tjiu, Y. Y. Xia, T. Liu, *ACS Appl. Mater. Interfaces* **2012**, *4*, 2242 – 2249; b) L. Zhang, X. Zhang, L. Shen, B. Gao, L. Hao, X. Lu, F. Zhang, B. Ding, C. Yuan, *J. Power Sources* **2012**, *199*, 395 – 401.

[92] C. L. Liu, K. H. Chang, C. C. Hu, W. C. Wen, *J. Power Sources* **2012**, *217*, 184 – 192.

[93] a) Y. Wu, S. Liu, H. Wang, X. Wang, X. Zhang, G. Jin, *Electrochim. Acta* **2013**, *90*, 210 – 218; b) L. Li, K. H. Seng, H. Liu, I. P. Nevirkovets, Z. Guo, *Electrochim. Acta* **2013**, *87*, 801 – 808.

[94] X. C. Dong, H. Xu, X. W. Wang, Y. X. Huang, M. B. C. Park, H. Zhang, L. H. Wang, W. Huang, A. P. Chen, *ACS Nano* **2012**, *6*, 3206 – 3213.

[95] W. Zhou, J. Liu, T. Chen, K. S. Tan, X. Jia, Z. Luo, C. Cong, H. Yang, C. M. Li, T. Yu, *Phys. Chem. Chem. Phys.* **2011**, *13*, 14462 – 14465.

[96] a) B. Qu, Y. Chen, M. Zhang, L. Hu, D. Lei, B. Lu, Q. Li, Y. Wang, L. Chen, T. Wang, *Nanoscale* **2012**, *4*, 7810 – 7816; b) S. Yang, X. Wu, C. Chen, H. Dong, W. Hu, X. Wang, *Chem. Commun.* **2012**, *48*, 2773 – 2775; c) X. Wang, S. Liu, H. Wang, F. Tu, D. Fang, Y. Li, *J. Solid State Electrochem.* **2012**, *16*, 3593 – 3602.

[97] L. L. Zhang, Z. Xiong, X. S. Zhao, *J. Power Sources* **2013**, *222*, 326 – 332.

[98] a) Y. Y. Yang, Z. A. Hu, Z. Y. Zhang, F. H. Zhang, Y. J. Zhang, P. J. Liang, H. Y. Zhang, H. Y. Wu, *Mater. Chem. Phys.* **2012**, *133*, 363 – 368; b) C. Ge, Z. Hou, B. He, F. Zeng, J. Cao, Y. Liu, Y. Kuang, *J. Sol-Gel Sci. Technol.* **2012**, *63*, 146 – 152.

[99] S. Chatterjee, A. K. Patra, A. Bhaumik, A. K. Nandi, *Chem. Commun.* **2013**, *49*, 4646 – 4648.

[100] a) D. W. Wang, F. Li, J. Zhao, W. Ren, Z. G. Chen, J. Tan, Z. S. Wu, I. Gentle, G. Q. Lu, H. M. Cheng, *ACS Nano* **2009**, *3*, 1745 – 1752; b) J. Xu, K. Wang, S. Z. Zu, B. H. Han, Z. Wie, *ACS Nano*, **2010**, *4*, 5019 – 5026.

[101] Q. Wu, Y. X. Xu, Z. Y. Yao, A. R. Liu, G. Q. Shi, *ACS Nano* **2010**, *4*, 1963 – 1970.

[102] J. W. Long, D. Bélanger, T. Brousse, W. Sugimoto, M. B. Sassin, O. Crosnier, *MRS Bull.* **2011**, *36*, 513 – 522.

[103] P. J. Hung, K. H. Chang, Y. F. Lee, C. C. Hu, K. M. Lin, *Electrochim. Acta* **2010**, *55*, 6015 – 6021.

[104] J. T. Zhang, J. W. Jiang, H. L. Li, X. S. Zhao, *Energy Environ. Sci.* **2011**, *4*, 4009 – 4015.

[105] B. G. Choi, S. J. Chang, H. W. Kang, C. P. Park, H. J. Kim, W. H. Hong, S. Lee, Y. S. Huh, *Nanoscale* **2012**, *4*, 4983 – 4988.

[106] H. Gao, F. Xiao, C. B. Ching, H. Duan, *ACS Appl. Mater. Interfaces* **2012**, *4*, 2801 – 2810.

[107] a) J. Yan, Z. Fan, W. Sun, G. Ning, T. Wei, Q. Zhang, R. Zhang, L. Zhi, F. Wei, *Adv. Funct. Mater.* **2012**, *22*, 2632 – 2641; b) H. Gao, F. Xiao, C. B. Ching, H. Duan, *ACS Appl. Mater. Interfaces* **2012**, *4*, 7020 – 7026.

[108] K. R. Lee, K. U. Lee, J. W. Lee, B. T. Ahn, S. I. Woo, *Electrochem. Commun.* **2010**, *12*, 1052 – 1055.

[109] Z. H. Wen, X. C. Wang, S. Mao, Z. Bo, H. Kim, S. M. Cui, G. H. Lu, X. L. Feng, J. H. Chen, *Adv. Mater.* **2012**, *24*, 5610 – 5616.

[110] X. Wang, C. Yang, P. Liu, *Synth. Met.* **2012**, *162*, 2349 – 2354.

[111] L. Hu, J. Tu, S. Jiao, J. Hou, H. Zhu, D. J. Fray, *Phys. Chem. Chem. Phys.* **2012**, *14*, 15652 – 15656.

[112] Y. Liu, R. Deng, Z. Wang, H. Liu, *J. Mater. Chem.* **2012**, *22*, 13619 – 13624.

[113] J. H. Liu, J. W. An, Y. X. Ma, M. L. Li, R. B. Ma, *J. Electrochem. Soc.* **2012**, *159*, A828 – A833.

[114] P. Si, S. J. Ding, X. W. Lou, D. H. Kim, *RSC Adv.* **2011**, *1*, 1271 – 1278.

[115] L. Mao, K. Zhang, H. S. O. Chan, J. S. Wu, *J. Mater. Chem.* **2012**, *22*, 80 – 85.

[116] N. A. Kumar, H. J. Choi, Y. R. Shin, D. W. Chang, L. M. Dai, J. B. Baek, *ACS Nano* **2012**, *6*, 1715 – 1723.

[117] S. Bose, N. H. Kim, T. Kuila, K. T. Lau, J. H. Lee, *Nanotechnology* **2011**, *22*, 369502.

[118] P. A. Mini, A. Balakrishnan, S. V. Nair, K. R. Subramanian, *Chem. Commun.* **2011**, *47*, 5753 – 5755.

[119] X. Yan, J. Chen, J. Yang, Q. Xue, P. Miele, *ACS Appl. Mater. Interfaces* **2010**, *2*, 2521 – 2529.
[120] H. Wang, Q. Hao, X. Yang, L. Lu, X. Wang, *Nanoscale* **2010**, *2*, 2164 – 2170.
[121] S. Biswas, L. T. Drzal, *Chem. Mater.* **2010**, *22*, 5667 – 5671.
[122] H. Wang, Q. Hao, X. Yang, L. Lu, X. Wang, *ACS Appl. Mater. Interfaces* **2010**, *2*, 821 – 828.
[123] K. Zhang, L. L. Zhang, X. S. Zhao, J. Wu, *Chem. Mater.* **2010**, *22*, 1392 – 1401.
[124] Jaidev, S. Ramaprabhu, *J. Mater. Chem.* **2012**, *22*, 18775 – 18783.
[125] X. M. Feng, R. M. Li, Z. Z. Yan, X. F. Liu, R. F. Chen, Y. W. Ma, X. A. Li, Q. L. Fan, W. Huang, *IEEE Trans. Nanotech.* **2012**, *11*, 1080 – 1086.
[126] Y. Liu, Y. Zhang, G. Ma, Z. Wang, K. Liu, H. Liu, *Electrochim. Acta* **2013**, *88*, 519 – 525.
[127] S. Zhou, H. Zhang, Q. Zhao, X. Wang, J. Li, F. Wang, *Carbon* **2013**, *52*, 440 – 450.
[128] X. Dong, J. Wang, J. Wang, M. B. C. Park, X. Li, L. Wang, W. Huang, P. Chen, *Mater. Chem. Phys.* **2012**, *134*, 576 – 580.
[129] N. A. Kumar, H. J. Choi, A. Bund, J. B. Baek, Y. T. Jeong, *J. Mater. Chem.* **2012**, *22*, 12268 – 12274.
[130] M. Xue, F. Li, J. Zhu, H. Song, M. Zhang, T. Cao, *Adv. Funct. Mater.* **2012**, *22*, 1284 – 1290.
[131] C. Z. Zhu, J. F. Zhai, D. Wen, S. J. Dong, *J. Mater. Chem.* **2012**, *22*, 6300 – 6306.
[132] F. Alvi, M. K. Ram, P. A. Basnayaka, E. Stefanakos, Y. Goswami, A. Kumar, *Electrochim. Acta* **2011**, *56*, 9406 – 9412.
[133] J. Li, H. Xie, Y. Li, J. Liu, Z. Li, *J. Power Sources* **2011**, *196*, 10775 – 10781.
[134] A. Davies, P. Audette, B. Farrow, F. Hassan, Z. Chen, J.-Y. Choi, A. Yu, *J. Phys.Chem. C* **2011**, *115*, 17612 – 17620.
[135] C. H. Xu, J. Sun, L. Gao, *J. Mater. Chem.* **2011**, *21*, 11253 – 11258.
[136] X. M. Feng, R. M. Li, Y. W. Ma, R. F. Chen, N. E. Shi, Q. L. Fan, W. Huang, *Adv. Funct. Mater.* **2011**, *21*, 2989 – 2996.
[137] L. L. Zhang, S. Zhao, X. N. Tian, X. S. Zhao, *Langmuir* **2010**, *26*, 17624 – 17628.
[138] H. Wang, Q. Hao, X. Yang, L. Lu, X. Wang, *Electrochem. Commun.* **2009**, *11*, 1158 – 1161.